Enhancement of Distribution System Resilience Through the Application of Volt-Var Regulation Devices

A Thesis

Presented in Partial Fulfillment of the Requirements for the

Degree of Master of Science

with a

Major in Electrical Engineering

in the

College of Graduate Studies

University of Idaho

by

Magdely Noguera

Major Professor: Brian K. Johnson, Ph.D.

Committee Members: Yacine Chakhchoukh, Ph.D., Ahmed Abdel-Rahim, Ph.D.

Department Administrator: Mohsen Guizani, Ph.D.

December 2017

AUTHORIZATION TO SUBMIT THESIS

This thesis of Magdely Noguera, submitted for the degree of Master of Science with a Major in Electrical Engineering and titled **"Enhancement of Distribution System Resilience Through the Application of Volt-Var Regulation Devices,"** has been reviewed in final form. Permission, as indicated by the signatures and dates given below, is now granted to submit final copies to the College of Graduate Studies for approval.

Major Professor: _____ Date: _____

Brian K. Johnson, Ph.D.

Committee Members: _____ Date: _____

Yacine Chakhchoukh, Ph.D.

_____ Date: _____

Ahmed Abdel-Rahim, Ph.D.

Department
Administrator:

_____ Date: _____

Mohsen Guizani, Ph.D.

ABSTRACT

Power distribution systems could potentially see high penetration of mixed distributed energy resources. This creates a need for new ways to analyze the electrical systems to assure a more resilient, reliable and strong power system. Nowadays, the typical power grid is designed to generate electricity in a dispatchable, centralized mode. The grid typically does not contain much, if any, energy storage capability. In addition to this, the distribution systems have been characterized as having predictable passive loads, without any generation, and largely fed by radial feeders, which means that the power flow is unidirectional from the distribution substations to the customers.

The last decade has seen a significant increase in application of renewable generation resources interconnected to both transmission and distribution systems, and this trend is accelerating. The mixed DERs are stochastics sources and are largely not-dispatchable, resulting in potential for power flow from the distribution levels to transmission grid. The incorporation of microgrids has been proposed, with some initial applications. In addition, loads have evolved into more active forms. All these changes make the control of the power grid more complex and add more functions and requirements to reach an optimal operation between all of the entities that make up the power grid of the future.

Maintaining or improving the resilience of a power grid will depend on the control of the assets connected into the grid. These assets can be classified as controllable and non-controllable. This thesis will focus on adding dynamic reactive power sources at pinch points in the distribution system to improve resilience. The scheme will be tested in a distribution model that is presented as an approximation of a possible electrical grid of the future. A method for sizing the reactive compensators will be presented and tested through simulation

looking at different levels of solar penetration. The optimal location and sizing of the D-STATCOMs aligned to the reactive power requirements will be analyzed for different scenarios. At the end, these results will provide data for the evaluation of resilient metrics of these systems.

On a different note, the application of PV systems has grown in the last years because of the carbon dioxide reduction needs and the growth of the electrical energy demand. Locations where the power grid is not accessible are the ideal to use this new source of energy, such cases are known as stand-alone system installations since they are not connected to the power grid. However, since the dependency on the daylight solar energy resource; many applications include batteries to provide electricity when the sunlight is not available. Therefore, an assessment of two types of solar cells will be included in this thesis to decide which of them will be more efficient to use for small stand-alone applications.

ACKNOWLEDGEMENTS

I would like to express my special gratitude to my advisor, Dr. Brian Johnson, for being my main support in this research and during all my Master studies. Your quality as a human being and your professionalism have inspired my life in a personal and professional way.

I extend my sincere thanks to Dr. Yacine Chakhchoukh and Dr. Ahmed Abdel-Rahim for serving on my committee and for providing indispensable advice, time and support towards the completion of this research. I would also like to thank Tim and Craig for their unconditional support and interest on this study.

Mike and John at the Electrical Engineering Department for being providing me with the required tools, equipment and software.

I feel blessed for my family and friends who always had positive advice and trusted in my knowledge and capacities to see this dream come true.

DEDICATION

I dedicate this work to my God; my parents Maria and Vicente; my son Marcelo; my brothers Magdy, Leonardo and Alexander and the rest of my lovely family, in special to my angel Michael.

TABLE OF CONTENTS

LIST OF FIGURES

LIST OF TABLES

LIST OF ABBREVIATIONS

FACTS	Flexible Alternating Current Transmission Systems
D-STATCOM	Distribution Static Synchronous Compensator
EU	Economic Units
MDS	Modern Distribution System
DER	Distributed Energy Resources
VER	Variable Resources
VVO	Volt-Var Optimization
IEEE	Institute of Electrical and Electronics Engineers
NREL	National Renewable Energy Laboratory
DSO	Distribution System Operator
EPS	Electric Power System
SAIFI	System Average Interruption Frequency Index
SAIDI	System Average Interruption Duration Index
GTO	Gate Turn-off Thyristor
IGBT	Insulated Gate Bipolar Transistor
PUD	Public Utility District

CHAPTER 1. INTRODUCTION

1.1 PROBLEM STATEMENT

This thesis is divided in two parts. The majority of the thesis is related to application of dynamic reactive compensation to improve distribution systems resilience in scenarios with high penetration of distributed resources. One chapter will discuss results from work performed related to a project to characterize photovoltaic cell behavior to evaluate their capability for a stand-alone application.

Nowadays the incorporation of DER in electrical power systems is becoming a rapidly growing trend. Potential problems with integration of DER into distribution networks was not taken seriously few years ago since the levels of penetration were not significant. However, this scenario changed and large numbers of DER are being connected at the distribution levels. Voltage regulation is the most important technical challenge that tends to limit the amount of penetration of DER into the distribution network. In addition to voltage regulation, challenges on power quality, electrical protection systems and stability of distribution networks are also arising [1]. The first part of this will look at improving resilience in these scenarios.

In addition to this, stand-alone systems have become popular to feed some smaller and isolated loads. However, PV cells are characterized as having very low efficiencies especially when tracking systems are not considered, which is the case of the PV systems tested in this thesis. The efficiency of most of PV cells is low, ranging from 2% to 20% depending on the material and structure of the device. A 40% efficiency could be reached by using multilayer solar cells [2]. Therefore, selecting a higher efficiency PV cell will assure a better utilization of the solar energy resource for stand-alone applications which are not connected to any main power grid. The final part of this thesis will address such an application.

1.2 PROPOSED SOLUTION

1.2.1 Volt/VAR Optimization

Traditional Volt/VAR Optimization (VVO) operates using on load tap changers (OLTC), switched capacitors (SC) and step voltage regulators (SVR) strategically located in distribution substations and along feeders [1]. Figure 1-1 shows the voltages drop in a distribution feeder from the substation to the customers. Since most distribution feeders are radial, the customers located at the end of the feeder tends to face lower service voltages than the others located close at the substation.

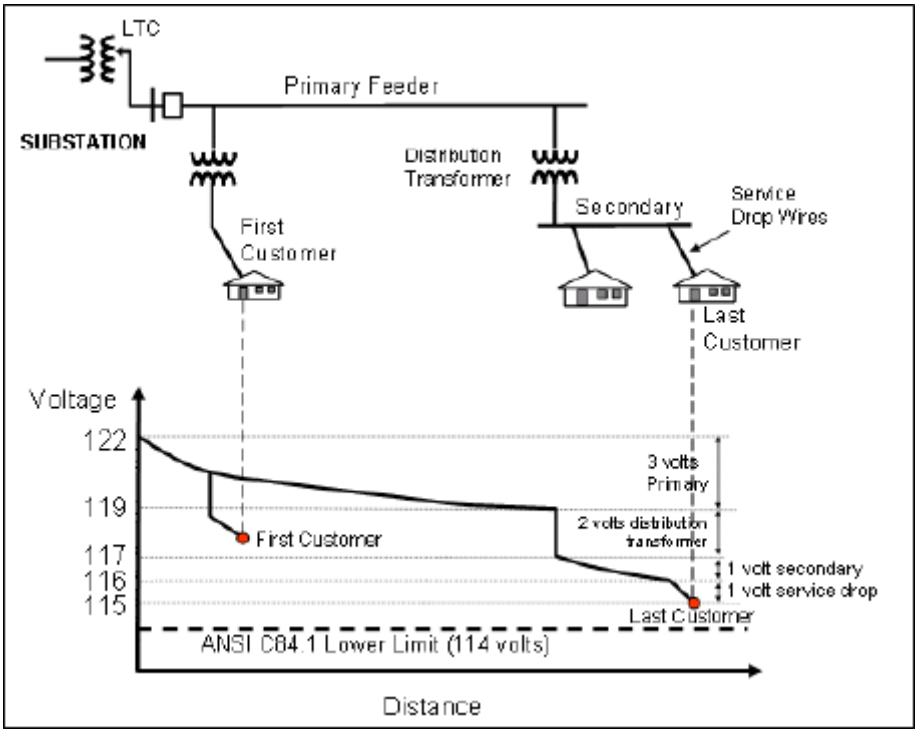

Figure 1-1 Voltage drops over a distribution feeder [3]

The disadvantages of SVRs and SCs are basically that SVRs are not capable of generating reactive power and SCs are unable to vary reactive power continuously and bring the risk of oscillatory behaviors by interacting with inductive elements of the grid. The application of power electronic devices in the family of devices once characterized as Custom

Power Devices can provide dynamic compensation of distribution systems to overcome many of the distribution network problems by reducing the line power losses, correcting power factor and improving the voltage profile of these systems. The D-STATCOM (Distribution STATCOM) behaves a shunt connected voltage source converter which provides strategic amounts of reactive power into the system, increasing the reliability and efficiency of the distribution systems [4].

1.2.2 PV Stand-alone Applications

Regarding to small PV systems to be used at small stand-alone applications, those will be characterized by their I-V curve to estimate the Maximum Power Point (MPP) during different seasons to follow the behavior of the output power obtained by two different solar panels.

1.3 OBJECTIVES OF THIS THESIS

The main objective of the thesis is to perform a study for establishing a method to compensate the reactive power of a Modern Distribution System (MDS) by using the impedance matrix (Zbus) approach. Additionally, the enhancement of the resilience of the electrical system needs to be proven by applying resilience metrics. The studies performed include:

a) Explore the Gridlad-D capabilities to apply voltage regulation on the primary distribution level (14.2 kV) of residential economic units.

b) Analyze the regulations regarding voltage regulation on the distribution systems such as standards ANSI C84.1 and IEEE 1547.

c) Simulate the effect of the D-STATCOM devices on distribution networks by proposing a methodology to evaluate the candidate buses for placement of D-STATCOMs and calculate the required reactive power to make a more optimal voltage regulation.

d) Analyze the voltage profile, losses and peak demand in the system once the D-STATCOM devices are added to the distribution network.

e) Evaluate the improvement of the system's resiliency by applying voltage regulation under different operational scenarios.

f) Test PV cells for small stand-alone applications.

1.4 LITERATURE REVIEW

1.4.1 The Evolution of Distribution Systems

Traditional grid operation is based on the following principles: generation is centralized, connected at the transmission level and dispatchable; the grid has essentially no energy storage capability; distribution dynamics are slower, and distribution can be treated as having a predictable passive load connected to transmission levels. At the distribution level real power flow is unidirectional from the distribution substations to the customers. Figure 1-2 points out the fundamental control paradigm for the 20th Century. The main principle of operation was based on the dynamic balancing of generation and load in a load-following manner by dispatching generation to meet the limits on system frequency and voltage levels [5].

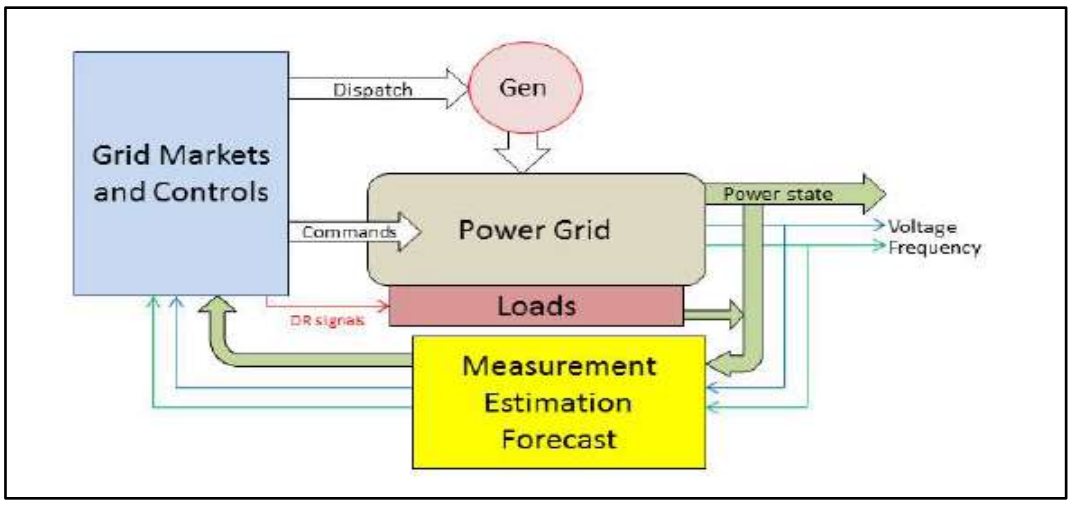

Figure 1-2 Fundamental control paradigm for the 20th century [5]

However, a variety of factors are changing the requirements for distribution grid operation. These include the high penetration of non-dispatchable generation sources, especially solar and wind; the increasing penetration of generation sources at distribution levels, with both dispatchable and non-dispatchable generation sources, also known as variable resources (VER); the growth of prosumers who are considered producer-consumers of electrical energy; the emergence of microgrids as isolated systems that can operate stand-alone during certain conditions for restricted period of time and to have high levels of reliability and resilience during natural disasters and human attacks or stresses on the grid. Microgrids can also interface to the power system as controlled aggregate loads or power sources.

A notable increase complexity is added to distribution systems because of the factors mentioned above. Some of these consequences include reducing total inertia of the bulk power system; increasing unpredictability of distribution system behavior leading to operability problems for maintaining power balance and stability between the loads and generation sources.

Additionally, the penetration of stochastic sources of generation demands fast-dynamic response of the distribution grid, increasing the need for control capabilities to improve resilience. In response to the emerging trends and resulting systemic issues, electric power distribution is being changed in a variety of ways. Overall, distribution is beginning to experience an evolution that will impact not just electric circuit technology, but also industry structure, business models, and regulation.

Figure 1-3 illustrates the evolving paradigm for grid control in the 21st Century, which comprises dynamic balancing of generation, combined load and DER in a hybrid source-and-load following manner that includes dispatch of some DER, and using storage and load reduction, subject to bounds on system frequency, voltage levels, and DER capacities [5].

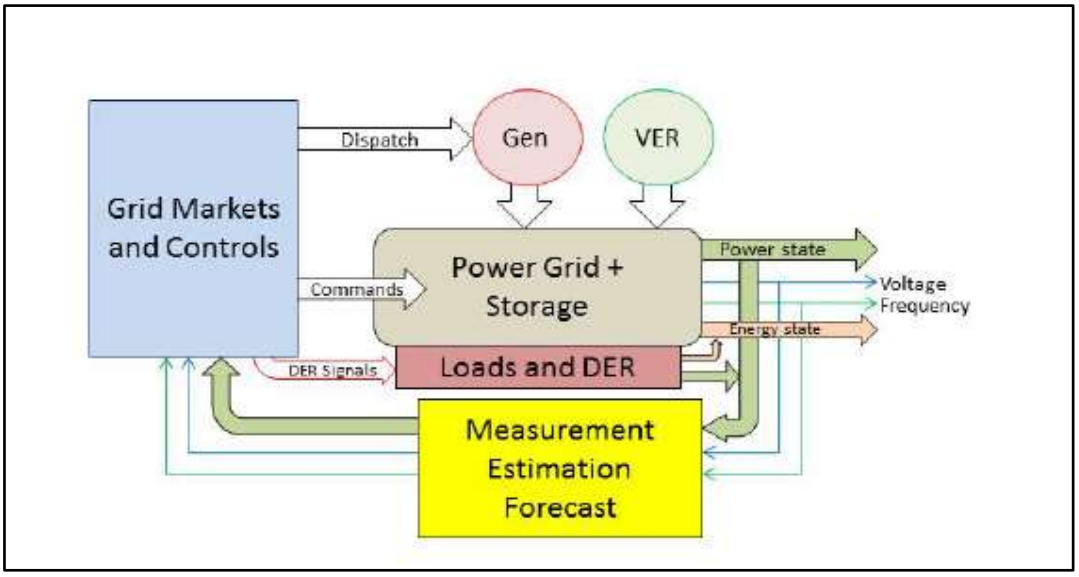

Figure 1-3 The evolving paradigm for grid control in the 21st century [5]

Dispatchable and non-dispatchable generation sources have been added into the distribution levels along with new capabilities for loads to be responsive; therefore, a new environment for distribution grid control is required to operate distribution systems properly by managing these new assets connected into the system. These new control schemes result

in algorithms which are more complex and only can be implemented by operating what are broadly called smart grid technologies.

1.4.2 Stages of Distribution System Evolution

Based on the aggregate growth of DERs into the current distributions systems, a three-stage evolutionary framework has been developed to explain the process of adoption of DER. In US the adoption of the DER is uneven, which means some areas have significant adoption while others have not incorporated these new technologies into the distribution systems. The adoption of DER is determined mostly by policies, technological cost-effectiveness, local economic factors and consumer interest. Figure 1-4 shows the three-stage evolutionary framework proposed in [6].

1.4.2.1 Stage 1: Grid Modernization

This stage represents the state of distribution utility grid modernization and reliability investments currently underway or soon to be made. In this stage, the level of customer DER adoption is low and can be accommodated within the existing distribution system without material changes to infrastructure or operations. Most distribution systems in the U.S. are currently at Stage 1 [6].

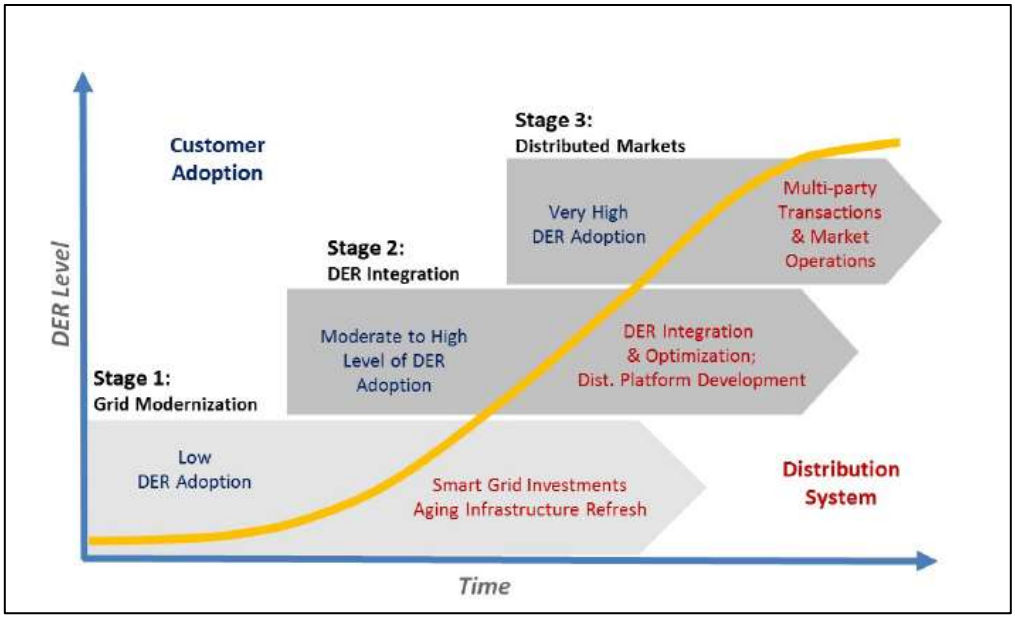

Figure 1-4 Distribution system evolution [6]

1.4.2.2 Stage 2: DER Integration

In this stage, DER adoption levels become higher until they reach a threshold level that requires enhanced functional capabilities for reliable distribution operation. In this stage the DERs might provide system benefits. Therefore, new changes on distribution planning and operations are needed. A five percent or more penetration of DER under peak loading condition tends to be defined as the Stage 2 DER adoption threshold based on DER adoption experience in US. In this stage there is a high customer adoption in neighborhoods and commercial areas. California and Hawaii are in Stage 2 based on DER adoption and public policy decisions [6].

1.4.2.3 Stage 3: Distributed Markets

This conceptual stage results from a combination of high DER adoption and policy decisions to create distribution-level energy markets for multi-sided (“many-to-many” or “peer-to-peer”) transactions. In Stage 3 DER is conceptually very well settled and the providers and “prosumers” might go beyond of their own electrical needs and decide to

provide services to the wholesale market and the distribution system. Energy transactions also are encouraged between these two sectors; therefore, institutional changes should allow retail energy transactions across the distribution system [6].

1.4.3 Volt-Var Control in Distribution Systems

1.4.3.1 Overview

The implementation of Voltage/VAR management or control is managed mainly by the electrical utilities companies which must deliver the electrical power to assure the voltage limit requirements are met for the appropriate operation of the customer's equipment, while also minimizing losses in the distribution infrastructure. However, voltages along distribution feeders are impacted by factors such as substation bus voltages, lengths of feeders, conductor sizing, types of loads, adoption of DER; among others. Since the electrical infrastructure of distribution systems is undergoing a severe transformation, more complexity is added continuously, making the task of managing electrical distribution networks more challenging [7].

As mentioned above, Volt/VAR control comprises voltage regulation and VAR regulation. The first focus is on feeder voltage regulation under varying load conditions. Utilities aim to deliver power to consumers within a predefined voltage range [7]. ANSI standard C84.1 [8] defines the limits to be followed for the service and utilization voltages. The Range A is related to normal operating conditions, this is; the service voltage levels range that comprised the original design and operational conditions. Range B is defined for those operational values that go beyond voltages level at Range A as a consequence of temporary abnormal operational conditions [9]. During high load, the voltage at the source end of the

feeder might be at the higher limit of the range A in order for the voltage at the far end of the feeder to be just above to the lower limit. [7].

The second control type, VAR Regulation, is related to the amount of VARs demanded by the loads in the system. Reactive power can be supplied by remote generators or local sources such as a capacitor bank. However, the flow of reactive power through the feeders increases the losses and voltage drop in the system. Therefore, during high demand of VARs in the system; utilities typically switch capacitors on during periods of high demand and switch them off during periods of low demand [7].

Since the flow of reactive power affects power system voltages, experience has proven that overall costs and performance of operating a power system can be best managed if voltage control and reactive power control are well integrated. For this reason, integrated Volt/Var control is one of the most desired functions for a modern Distribution Automation (DA) system [10].

1.4.3.2 Conservation voltage reduction (CVR)

Conservation voltage reduction (CVR) is an advanced strategy that reduces real power demand by lowering customer voltages within approved limits. CVR controls feeder and substation equipment to lower distribution line voltage within the approved standard ranges. The result is a significant reduction of losses and energy demand. They can also change target objectives at different times of the day/week/month/year to meet performance goals [11].

This type of VVO solution can be used to flatten voltage profiles and then lower overall system voltage while staying within the specified ANSI voltage limits. The result of doing this is an overall system demand reduction by a factor of 0.7-1.0% for every 1% reduction in voltage. From a consumer point of view, CVR reduces the energy that they

consume and pay for. From a utility point of view, the amount of power that they generate or purchase from outside generation stations is reduced. Therefore; the benefit associated with reduced operating costs, can be implemented to invest on new generation capacity or other beneficial assets for the distribution systems [7]

1.4.3.3 Volt-Var Control Demonstration Projects

Some projects which applied the concept of VVC are the following:

a) The Snohomish County PUD installed a Conservation Voltage Reduction system to improve system efficiency and improve power quality. The investment total was under $5 million, and the resulting energy savings were about 53,856 MWh/yr, including reducing distribution system losses by 11,226 MWh/yr while providing better voltage quality to end-use customers [7].

b) The Northwest Energy Efficiency Alliance studied 13 utilities for the impact of lower voltage on consumers. Their work showed voltage reductions of 2.5% resulted in energy savings of 2.07% without impact on consumer power quality [7].

c) The Clinton Utilities Board used state-of-the-art voltage regulation technologies to power 3,000 homes solely through energy savings. The Utilized Dispatchable Voltage Regulation to safely and automatically adjust end-use voltages to meet peak demand needs [7].

d) Oklahoma Gas & Electric (OG&E) implemented a volt/VAR optimization (VVO) across 400 feeder circuits to achieve a 75-megawatt load reduction. Advanced model-based VVO allowed OG&E to maximize the performance and reliability of its distribution systems while significantly reducing peak demand, minimizing power losses and lowering overall operating costs [7].

1.4.3.4 Volt-Var Control Benefits

The main benefits of VVC for distribution system are [12] [3]:

a) Improved energy efficiency leading to reduced greenhouse gas emissions.

b) Reduced peak demand and reduced peak demand cost for utilities.

c) Improved voltage profile.

d) Reduced numbers of tap changer operations.

1.4.3.4 Volt-Var Control Challenges

The main technical issue is to determine the optimal solution to apply VVC to distribution feeders. The communication technology is a key component as well as the optimal sensing solutions to provide real-time voltage measurements for the VVC system [7]. Another challenge to application of VVC on the distribution feeders is high penetration of DERs. Due to bi-directional flow of power, DERs tend to raise the voltage at the point of common coupling (PCC) and at the neighboring buses. Consequently, regulating the voltage through distribution feeders with high DER needs more advanced strategies [1].

Finally, it is important to mention the financial hurdles to the deployment of VVC schemes. Utilities, are paid by the electric power that is delivered to the customers; in the majority of cases they have limited incentives to implement energy savings schemes [7].

1.4.4 Voltage Regulation Standards

1.4.4.1 ANSI C84.1

The most commonly applied steady-state voltage standard in the United States is ANSI C84.1-2016 [8]. Within the standard, steady-state service voltage requirements are defined in two categories for medium voltage installations:

1. Range A is for normal conditions and the required regulation is from -2.47% to +5% (0.975 to 1.05 on a per unit basis).

2. Range B is for abnormal conditions and is intended to be for events that are limited in quantity and duration. The allowable range for these conditions is -5% to +5.21% (0.95 to 1.052 on a per unit basis).

1.4.4.2 IEEE 1547 Series Guidelines

The Institute of Electrical and Electronics Engineers (IEEE) Recommended Practice Standard 1547 [13] has been a foundational document for the interconnection of distributed energy resources (DER) with the electric power system or the grid. This standard is unique as the only US National Standard addressing systems-level DER interconnected with the distribution grid. IEEE 1547 was released in 2003. If a utility chooses to apply IEEE 1547, all types of DER connected into the grid must meet the outlined requirements at their point of common coupling. With the increase in cases where DER are involved, a series of guidelines were developed to build on the first standard. The 1547 series of standards as of 2014 are outlined in Figure 1-4 [12].

Figure 1-5 IEEE 1547 series of interconnection standards [12]

The draft document P1547.8 recommends practices to address expanded use of 1547 through the identification of innovative designs, processes, and operational procedures. P1547.8 addresses advanced controls and communications for inverters supporting the grid and best practices addressing multiple inverters and microgrids, and provides state-of-the-art information for DER group behavior and interactions with grid equipment and interconnection system response to abnormal conditions, and provides application examples such as state-of-the-art protection practices and advanced approaches to handle unintentional islanding [12].

The IEEE Standard 1547a (year 2014) Amendment 1 to 1547 was published in May 2014 [12]. Since 1547 was published in 2003, there have been significant developments of new interconnections, and lessons were learned, and additional engineering best practices were established based on the real-world implementation, including Smart Grid advances. In

mid-2012, IEEE 1547 officials held a workshop for revision of 1547, resulting in the consensus to first establish an amendment to 1547 addressing the top three highest priorities from the workshop—voltage regulation, voltage ride through, and frequency ride through. The IEEE ballot draft was completed in June 2013. The 1547 Amendment 1 now allows DER to support grid voltage regulation and provide voltage and frequency ride through. Amendment 1 is applicable to all of the original types of DER stated in 1547—static power inverters and converters, induction machines, and synchronous machines [12].

In Amendment 1, the operators of the distribution grid and the DERs are required to coordinate and approve when the DER can actively participate in voltage regulation by changes to real and reactive power. The manufacturer specifies the characteristics of its equipment as to how it will respond to provide changes in its real and reactive power output to support the grid. Generally, the equipment could respond autonomously to variations in grid voltage, via communicated settings, or via a time schedule. This allowable advanced functionality will provide a more robust grid and can be inherently integrated with utility grid operating practices.

Similarly, in Amendment 1, under mutual agreement between the operators of the grid and the DERs, the DER is permitted much wider latitude in how it responds to abnormal voltage and frequency conditions, including that DER are now clearly allowed to provide voltage and frequency ride through. The required voltage and frequency equipment functionalities are greatly expanded in the Amendment and the operational flexibility is enhanced [12].

1.4.5 Optimal Placement and Sizing of D-STATCOM

Custom power devices can play an important role to solve problems related to the reduction of line losses, correction of power factor and improvement of the voltage profile of the system. Many research papers have been developed regarding to the optimal location and sizes of custom power devices [4]. In [4] an optimal placement of D-STATCOM in a distribution mesh by using sensitivities indices is proposed. Fast Voltage Stability Index (FVSI), Combined Power Loss Sensitivity (CPLS), Voltage Stability Index (VSI), Voltage Sensitivity Index (VSEI) and authors Proposed Stability Index (PSI) were studied for a UK 38-bus mesh distribution system with realistic 24 h time varying load without and with D-STATCOM. Optimal D-STATCOM sizes are given for seasonal loads. The location recommendation for the D-STATCOM were better from the CPLS and the authors SI compared to those obtained for the other indices. With the D-STATCOM, there was significant improvement in the voltage profile, an enhanced voltage stability margin and reduction in power losses.

In addition to these methods in [4], proposed immune algorithms, particle swarm optimization algorithms, firefly algorithms, bacterial foraging optimization algorithms and harmonic search algorithms are some of the other methods developed for optimal location and sizing of D-STATCOM [4].

1.4.4 Power Grid Resilience

Resilience defines the ability of a system to respond to unexpected disturbances while maintaining an acceptable operating state [15]. In [16] the term resilience is used to describe the ability of the distribution system to adapt depending on the assets available in the system. The Disturbance and Impact Resilience Evaluation Curve (DIREC) shown in Figure 1-6,

describes the ability of a system to maintain minimal normalcy and the temporal measures of recovery to disturbances.

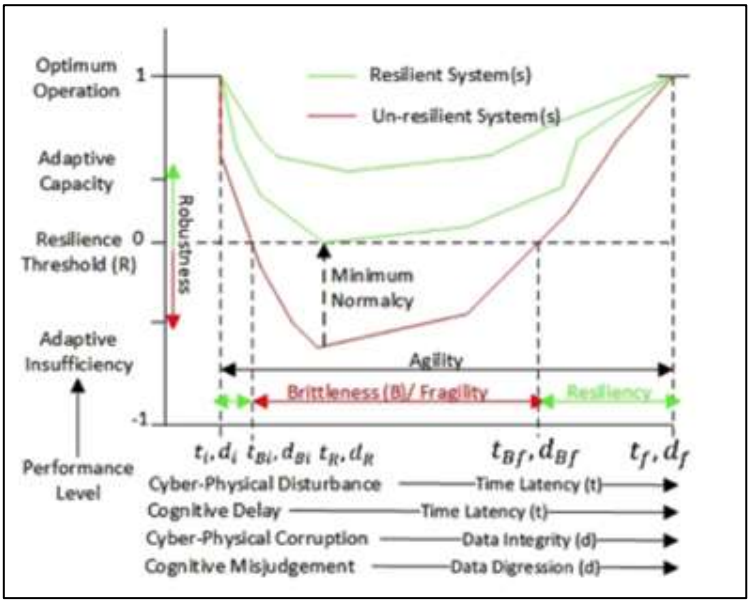

Figure 1-5 Disturbance and Impact Resilient Evaluation Curve (DIREC) [4]

For a better understanding of the DIREC curve the following concepts need to be explained with more detail [17]:

a) Agility: the ability of the system to resist disturbances as well as the rate of recovery toward acceptable operational conditions.

b) Robustness: It could be a positive or negative number associated with the area between the disturbance curve and the resilience threshold that could indicate either the capacity or insufficiency.

c) Adaptive Capacity: A value between 0 and 1 which represents the ability of the system to adapt to or transform from an impact and maintain minimum normalcy.

d) Adaptive Insufficiency: A value between 0 and -1 which represents the inability of the system to adapt or transform from impact, indicating unacceptable operation in the system in response to disturbances.

e) Brittleness: The area under the disturbance curve as intersected by the resilience threshold. This indicates the impact from the loss of operational normalcy.

f) Resiliency: The converse of brittleness, which for a resilience system is "zero" loss of minimum normalcy.

Traditional power system reliability metrics such as System Average Interruption Duration Index (SAIDI) and System Average Interruption Frequency Index (SAIFI) assess the severity of past system failures to suggest areas for improvement. Resilience metrics improve upon this by providing situational awareness by estimating the future difficulty of maintaining minimum normalcy in real time [15].

One example of evaluating resilience related to a MDS is shown in [15] where the pinch points were defined as those points in the system where the generation moves in an opposite direction to the load demand. By identify these points, corrective actions can be applied, such as the variation of power flow between nodes or the connection of energy storage devices into the system. As it is shown in Figure 1-6, at 18:00:00 it is seen that the load of the system is increasing, and the DG output is decreasing. In this case input from outside generation was increased to feed the load. By applying dispatchable generation actions, the minimum normalcy of the system can be maintained.

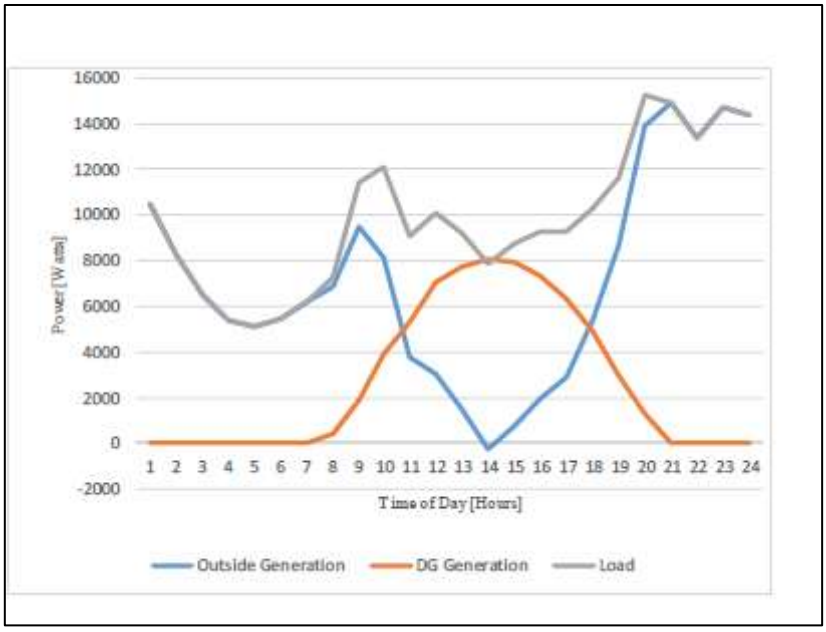

Figure 1-6 Pinch Points for a Residential Prosumer [15]

1.5 ORGANIZATION OF THIS THESIS

Chapter-1 of this document introduced the problem statement and the proposed solution. A literature review summarizes about the traditional voltage regulation techniques and introduce the new techniques available for future distribution systems. The benefits of voltage regulation on the distribution networks also are explained.

Chapter-2 describes the main characteristics of the example distribution model which contains four economic units (EU), residential, urban, rural/agricultural and industrial. The GridLAB-D software capabilities are described along the generation capability of the DER and seasonal load behavior for the residential EU.

Chapter-3 discusses basic concepts about the Voltage Regulation and Resilience and applied to distribution networks. In addition, details about traditional and modern equipment to compensate reactive power used in traditional and modern systems will be discussed. A method to regulate voltage in the system will be proposed and the scenarios to be analyzed will be define defined.

Chapter-4 presents the simulation results and the analysis for each studied case. Tables and graphics will provide visualization for each scenario.

Chapter-5 describes theory related to modeling PV solar panels and the Maximum Power Point Tracking (MPPT) options. The Maximum Power Point (MPP) for two types of solar panels related to a small stand-alone lighting application are compared to evaluate which of those is more efficient through the different seasons of the year.

Chapter-6 presents conclusions and future possible work, including proposed ideas that are useful for the implementation of voltage regulation techniques with high DER penetration.

Appendix-A lists system data.

CHAPTER 2. CHARACTERISTICS OF THE PROPOSED SYSTEM

2.1 DISTRIBUTION SYSTEM MODELING

Traditionally most electrical analysis has been focused at the transmission levels [19]. In the last 20 years distribution system analysis has gained more importance with the emergence of technologies designed to operate at the distribution level including DER. Therefore, more detail about the distribution equipment modeling and DER was needed to obtain better control for real-time operation of these MDS. The differences between modeling distribution systems as opposed to transmission systems include the following [19]:

- More detail modeling of end-user load behavior.
- Operation of single phase lines and some infrequent double phase lines.
- Most feeders are radial.
- Loads are unbalanced.
- The R/X ratio on distribution systems are much higher than on transmission systems.

2.2 GRIDLAB-D SOFTWARE

Distribution specific analysis tools have been developed. This project uses GridLAB-D. GridLAB-D is a time series power distribution system simulation and analysis tool that provides information to users who design and operate distribution systems, and can be used by utilities to evaluate the latest energy technologies. It incorporates advanced modeling techniques with high-performance algorithms to deliver the latest in end-use load modeling technology [23].

GridLAB-D was developed by Pacific Northwest National Laboratory (PNNL) in collaboration with industry and academia through funding from the U.S. Department of

Energy Office of Electricity Delivery and Energy Reliability (DOE/OE). GridLAB-D is designed as an open-source tool with the intent that numerous people and organizations will participate in the development of this tool to capture the complexity of the emerging smart grid technologies. GridLAB-D can be downloaded at [23].

As an agent-based simulation environment, GridLAB-D is designed to model not only the power system but also the systems that affect the power system. This allows the ability to track the detailed interplay between all the elements over time all the way from the substation to the end-user load [23].

2.1.1 GridLAB-D Capabilities

With the ability to perform time series simulations to evaluate the behavior of MDS behavior, GridLAB-D integrates the interactions between physical phenomenon, business systems, markets and regional economics, and customer interactions to provide a notion of how these subsystems affect the power system. GridLAB-D supports the following functions for electrical systems:

- 3-phase, unbalanced (meshed or radial) power systems,
- End-use load behavior of thousands to millions of homes and appliances,
- Retail level markets and transactive controls,
- Distributed generation and storage,
- Demand response and direct load control,
- Distribution automation controls, and
- Reliability analysis.

2.1.3 Power Flow with GridLAB-D

There are two modules in GridLAB-D to run power flow computations. The first is the power flow module designed to work with distribution systems and the second is called network module which works with transmission systems.

For the power flow module, the initial release of GridLAB-D implemented the well-established Forward Backward Sweep (FBS) algorithm. However, this algorithm does not readily permit analysis of systems that are meshed. Therefore, the incorporation of a networked solver was needed. A Newton-Raphson based current injection method (TCIM) [20] was implemented into the GridLAB-D to solve meshed systems [19]. To display voltage magnitude and angle, the real and imaginary part of the voltages at every node are computed [19].

2.3 SYSTEM TOPOLOGY

The proposed study system represents an area which is divided into four types of distribution systems: urban, residential, industrial and rural/agricultural. These four classes allow analysis of the behavior of future electrical systems [15].

The urban core is modeled by using meshed or semi-meshed feeders with time varying critical loads and prosumers. The prosumers are the producer-consumers who might generate electricity to the power grid at times and at other times consume power from the point of interconnection with the utility company. Conversely, the residential area contains only radial feeders, but also with flexible loads and smaller DG [15].

The rural system is characterized with sparse loading with longer feeders and larger concentrated DG generation, and also radial to semi-meshed feeders. The industrial system has a significant variety of loads connected to the feeders and the DG penetration is smaller. The topology is radial to semi-meshed [15].

The whole system is shown in the Figure 2-1, where normally open switches or reclosers are shown highlighted in green.

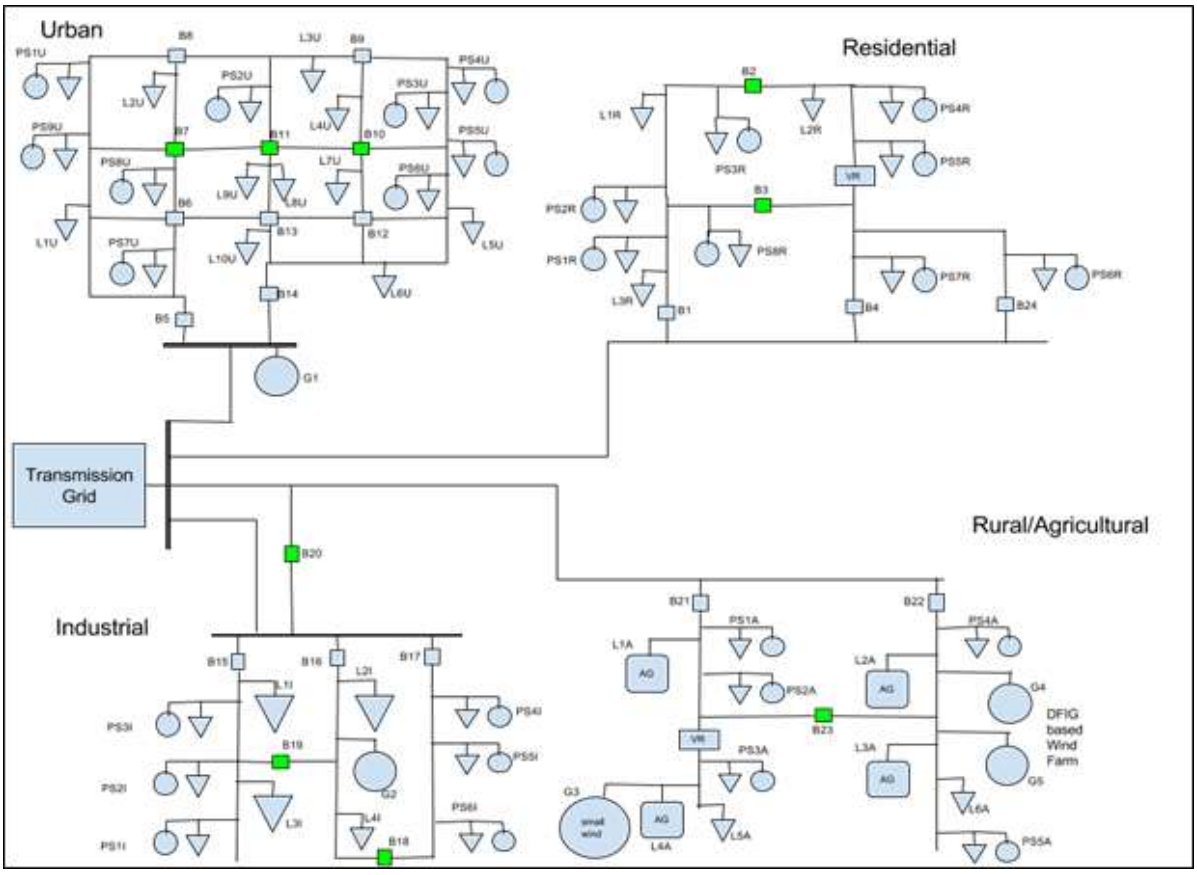

Figure 2-1 System topology [15]

2.4 RESIDENTIAL ECONOMIC UNIT

2.4.1 Generation Capability of the DER

The generation of electricity for the residential area will be provided largely by the electrical power coming from the bulk transmission system, which could be from traditional or not traditional sources, with some power from DER at prosumers.

The prosumer's generation is mainly solar generation for this system. The climate module in the GridLAB-D processes hourly weather data conditions which are commonly available from input files known as TMY2 and TMY3. TMY stands for "typical meteorological year." TMY2 is an older version with more limited geographic coverage, TMY3 supports more geographic location coverage with over 1000 locations in the United States. In addition, TMY3 supports more conventional csv format. The National Renewable Energy Laboratory (NREL) provides the weather condition data to estimate the solar generation resources [21].

The solar generation output depends mainly on the TMY files, array size and solar cell efficiency [15]. Figures 2-2 to 2-5 show the generation profile from solar energy for prosumers during a sample 24-hour period for four different seasons. The PV systems were modeled using the solar object and inverter object in GridLAB-D. For this thesis the inverters related to solar generation were set to operate in the constant PF mode. Therefore, the complex power obtained from the prosumers is only active power, expressed in kW.

The output for the solar generation from prosumer PS1R is shown in Figure 2-2. The same curves are applicable to prosumers PS4R, PS5R and PS7R. Figures 2-3 through 2-6 show the curves for prosumers PS2R, PS3R, PS6R and PS8R.

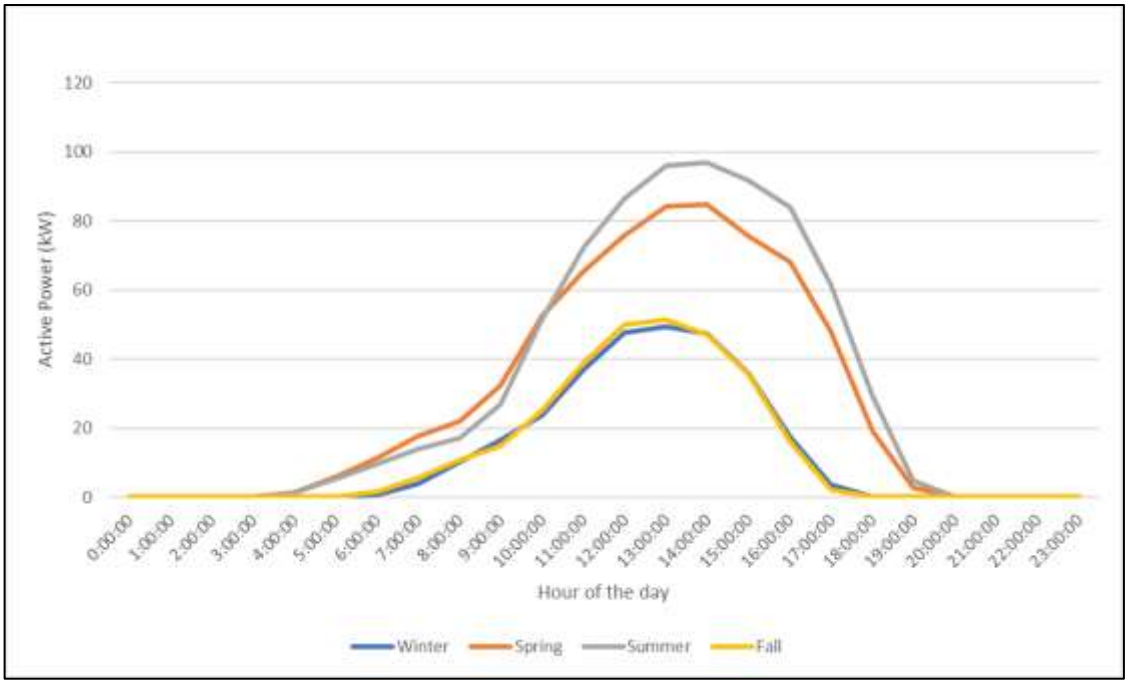

Figure 2-2 Average generation output profile of PS1R over sample 24-hour periods in 4 seasons

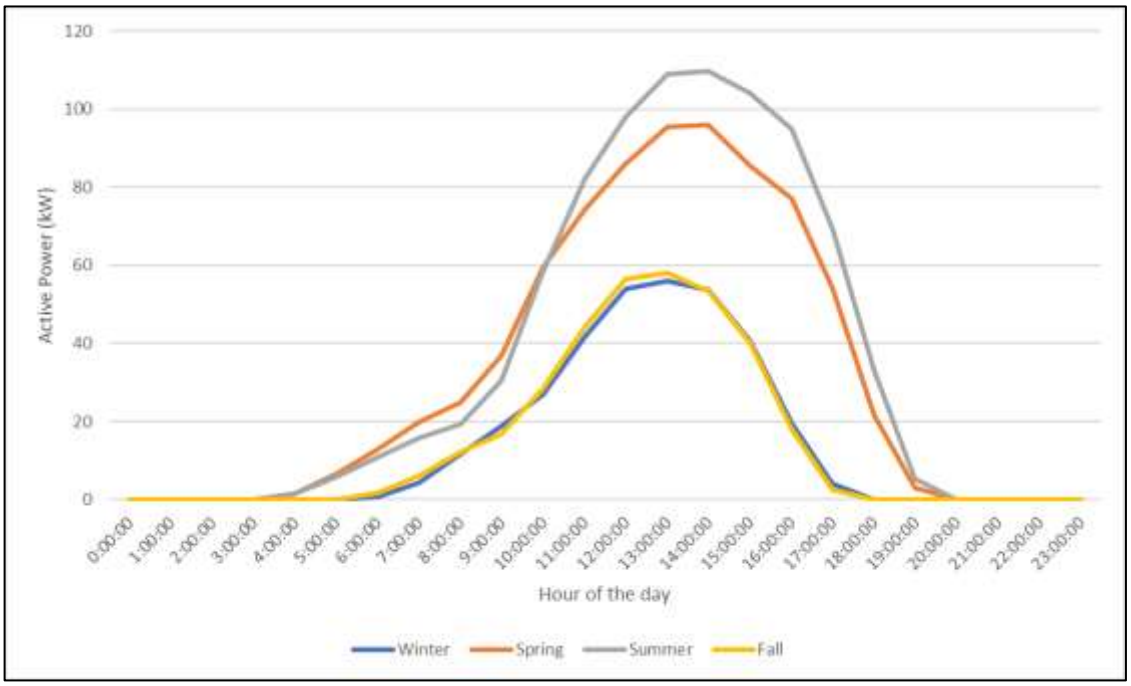

Figure 2-3 Average generation output profile of PS2R over sample 24-hour periods in 4 seasons

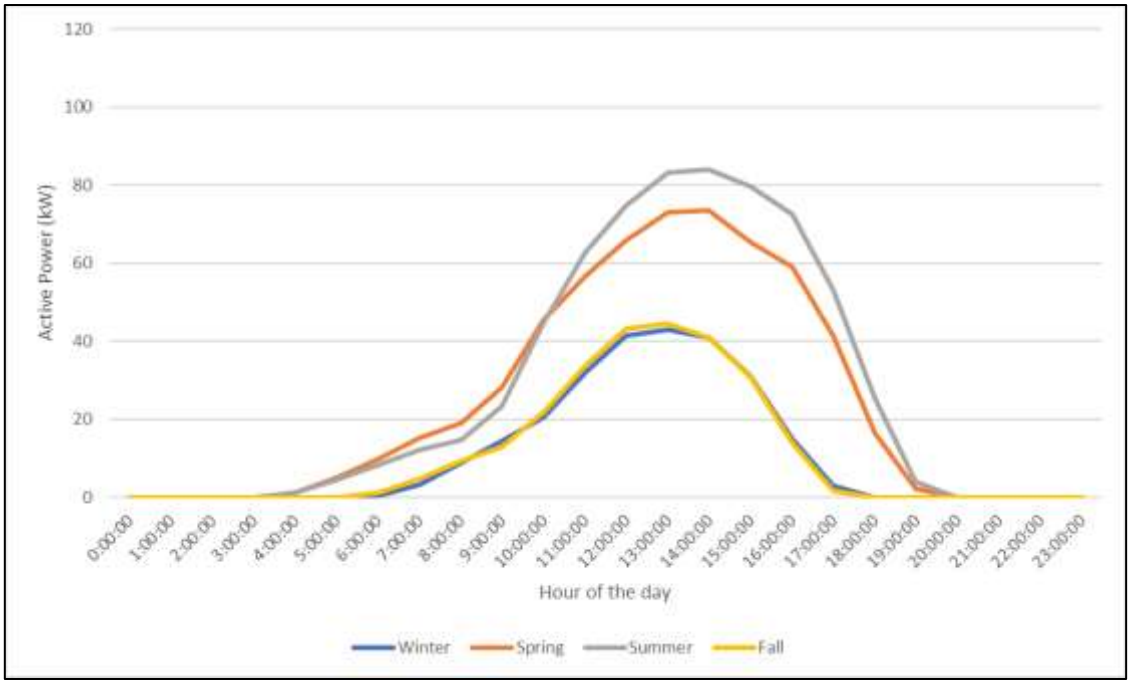

Figure 2-4 Average generation output profile of PS3R over sample 24-hour periods in 4 seasons

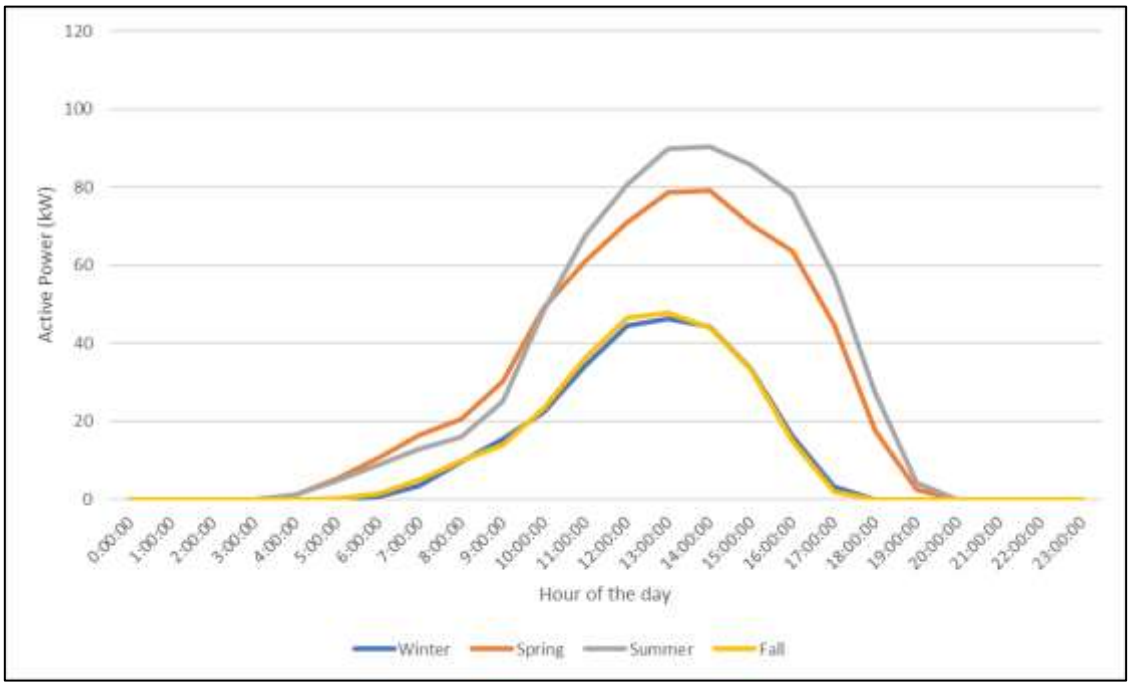

Figure 2-5 Average generation output profile of PS6R over sample 24-hour periods in 4 seasons

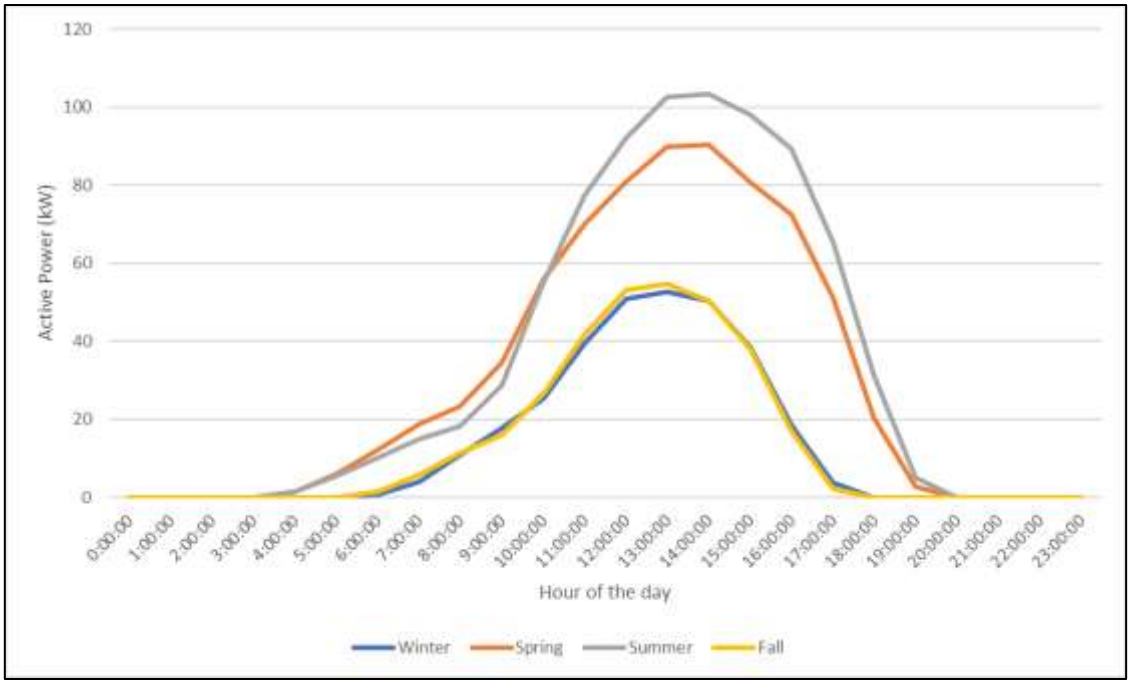

Figure 2-6 Average generation output profile of PS8R over sample 24-hour periods in 4 seasons

The incident solar radiation on a tilted PV array is calculated using classical formulas, implemented in built-in GridLAB-D models. The calculation involves various amounts of irradiance adjusted for time of day, the site latitude, orientation, and tilt angle of the PV panels [15]. The rated solar output is showed at Table 2-1, which was defined as an approximate value of the maximum annual solar output considered in this project. The specified period for the data set for the simulations is from 2009-01-01 to 2009-12-31. The Table 2-1 also indicates the scaling factor or level of penetration that was defined as the ratio between the nominal load and the amount of solar generation available for each prosumer.

Table 2-1: Prosumer solar generation characteristics

PV array	Scaling Factor	Nominal Power Output Solar (kVA)	Area Solar (ft^2)	Inverter Size (kVA)
PS1R	90%	170	15,000	15,000
PS2R	114%	190	17,000	20,000
PS3R	86%	150	13,000	4,000
PS4R	88%	170	15,000	20,000
PS5R	67%	170	15,000	20,000
PS6R	80%	160	14,000	20,000
PS7R	71%	170	15,000	20,000
PS8R	133%	180	16,000	5,000

2.4.2 Load Modeling and Seasonal Behavior

To more realistically model interactions between DERs and loads, time-varying load model with seasonal behavior were used. Load data was available in the NREL download site "Commercial and Residential Hourly Load Profiles for all TMY3 Locations in the United States" dataset [22]. Since only active power was included in this dataset, reactive power was calculated by assigning typical power factors according to the load type [15]. Once the load information was defined, a residential load player was created in GridLAB-D to simulate the annual load variation at the nodes with connected loads in the residential area topology. Figures 2-7 and 2-8 show typical seasonal load behavior during sample 24-hour periods for a single load connected in the system. Figures 2-9 and 2-10 point out the total seasonal load behavior during sample 24-hour periods for all of the loads connected in the system.

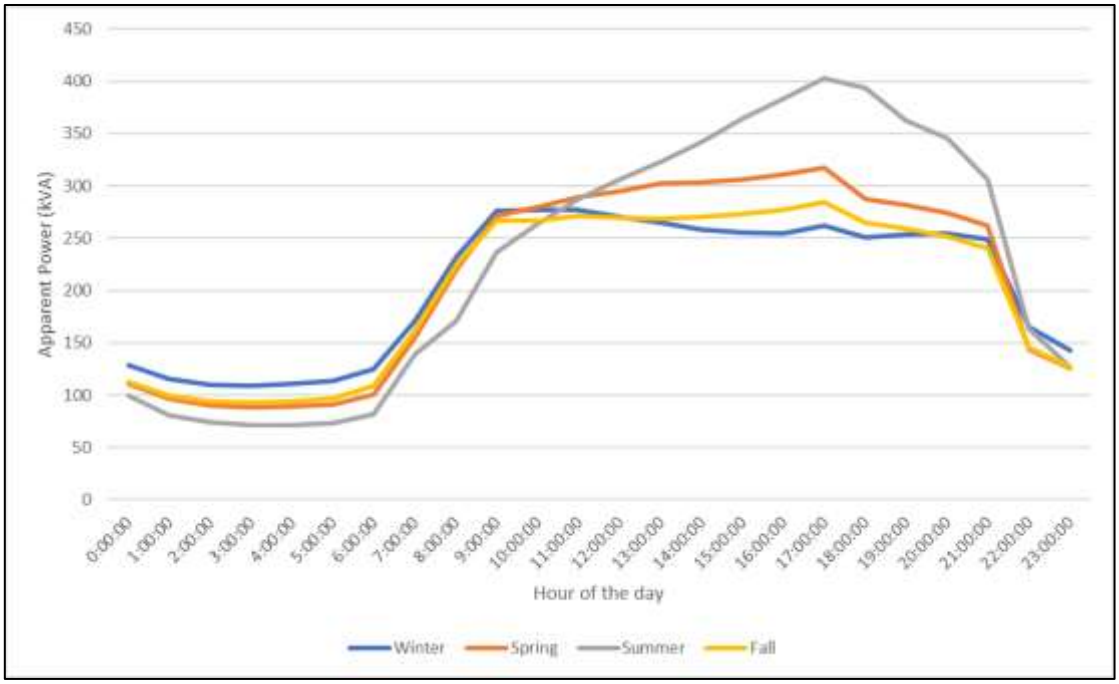

Figure 2-7 Average load demand over sample 24-hour periods in 4 seasons in kVA

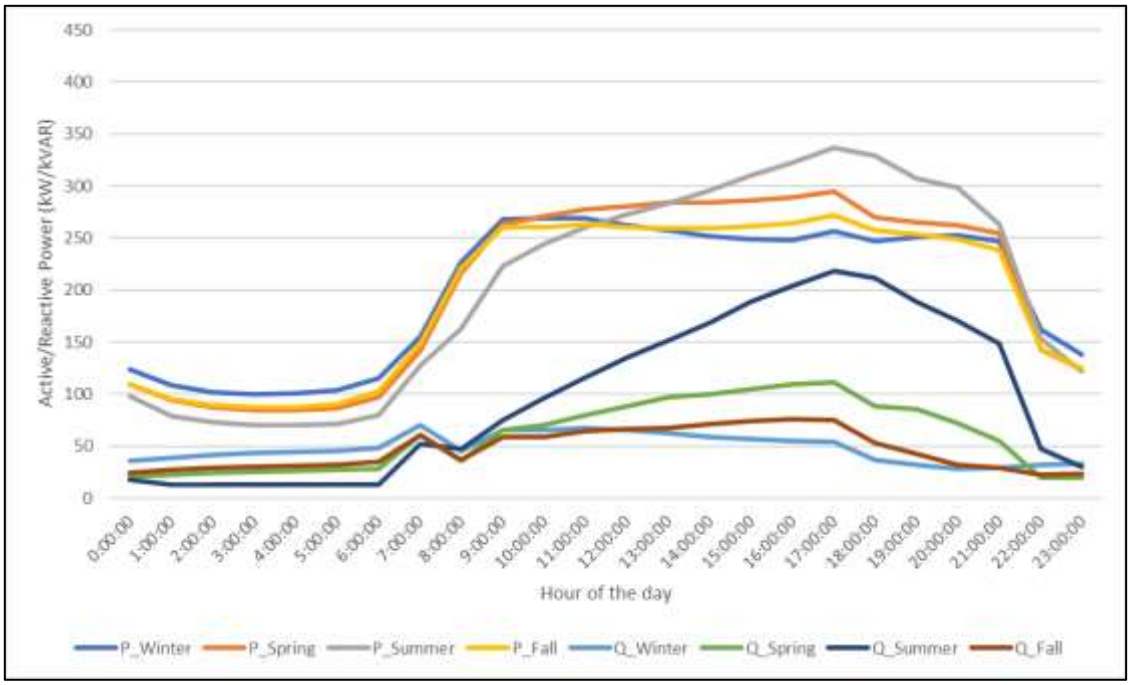

Figure 2-8 Average load demand over sample 24-hour periods in 4 seasons in kW/kVAR

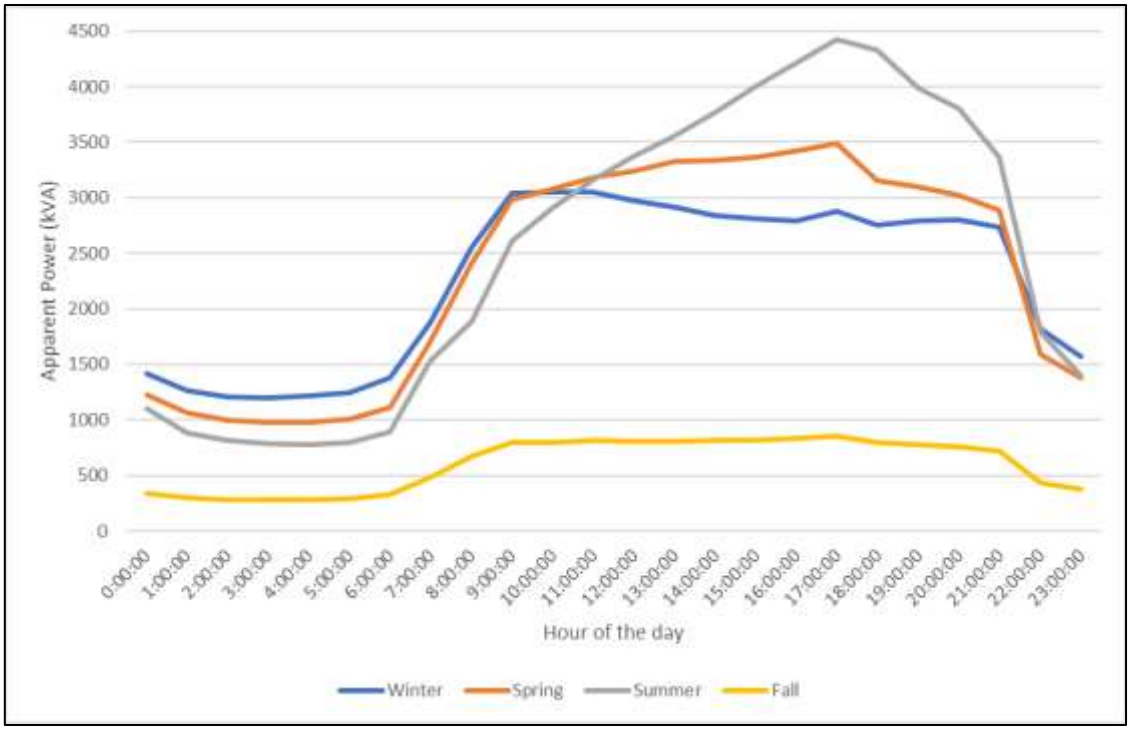

Figure 2-9 Average total load demand over sample 24-hour periods in 4 seasons in kVA

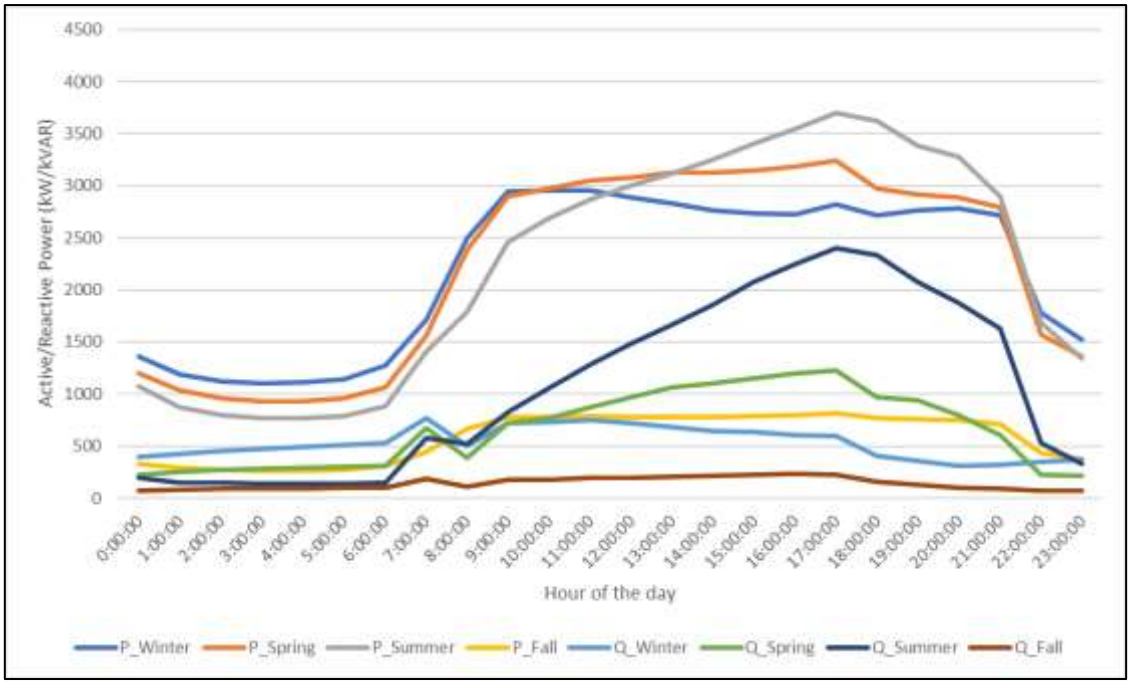

Figure 2-10 Average total load demand over sample 24-hour periods in 4 seasons in kW/kVAR

CHAPTER 3. VOLTAGE REGULATION AND RESILIENCE

3.1 DISTRIBUTION SYSTEM VOLTAGE REGULATION

Automatic voltage regulation of distribution systems is tipically provided by applying one or more of the following methods [24]:

- Bus voltage regulation at substation transformer
- Individual feeder regulation in the substation
- Supplementary regulation along the feeders

3.1.1 Substation bus regulation

A distribution substation transformer is commonly equipped with an Under Load Tap Changer (ULTC) which automatically controls the voltage in the secondary side. Another option it is to use a separate bus voltage regulator to regulate the secondary side bus voltage. A conventional transformer with an ULTC executes two functions: voltage transformation and voltage control [24].

3.1.2 Feeder bus regulation

Feeder voltage regulators control the voltage of each feeder. When there are several feeders with similar characteristics, they might be grouped to be controlled by a common regulator. In cases where the feeders are very long, it will be necessary to add other regulators and shunt capacitors at strategic points along the feeder to provide supplementary regulation [24].

3.1.3 Traditional Equipment

3.1.3.1 Under Load Tap Changer (ULTC)

An ULTC is a tap changing transformer. It adjusts its taps automatically to adjust the voltage by measuring the feeder current at the substation end of the line and estimating the voltage drop along the distribution feeder [1].

3.1.3.2 Step Voltage Regulator (SVR)

A step voltage regulator consists of an autotransformer with a LTC mechanism. The position of the tap is defined by a control circuit know as line drop compensator. Standard SVRs are equipped with a reverse switch which allows a ±10% of voltage regulation range, usually in 32 steps. Each step represents a 5/8% change in voltage [9]. Compared with ULTC, SVR perform only voltage control since they buck or boost the voltage without changing the basic voltage level [24].

3.1.3.3 Shunt Capacitors

Shunt capacitors (SC) are reactive power compensation devices characterized by providing reactive power and voltage support. From the point of voltage stability, shunt capacitors extend the voltage stability limits by correcting the power factor. However, shunt capacitors have the following limitations [24]:

- In heavily shunt capacitor compensated systems the voltage regulation becomes complicated to analyze and unpredictable in practice.
- Since the reactive power provided by the capacitor is proportional to the square of the voltage, the VARs support drops significantly during low voltage conditions.

3.1.4 Modern Volt-Var Regulation

The integration of DERs potentials makes the distribution power flow bi-directional and the voltage profile will depend on DERs location, injection of active power and power factor. Therefore, the overall situation through the feeder becomes unpredictable and it cannot be controlled by the ULTC. Additionally, due to the intermittent output nature of renewable DERs and the varying dynamic behavior of loads; the voltage variations occur so rapidly that traditional ULTCs or SCs cannot regulate as fast as required [1]. Therefore, new modern devices are required to overcome this challenging problem. The devices used in this thesis are the D-STATCOM and smart inverters in PV installations.

3.1.4.1 D-STATCOM

A D-STATCOM is a voltage source converter with no source or load on the DC bus [2]. The control of reactive power in the STATCOM is done by controlling its terminal voltage. Figure 3-1 shows a simplified circuit in which the ac grid is represented by a voltage source, $V_{S,}$ behind an impedance, $X_{L,}$ and the D-STATCOM is regulating a fundamental voltage, $V_{I.}$ [26].

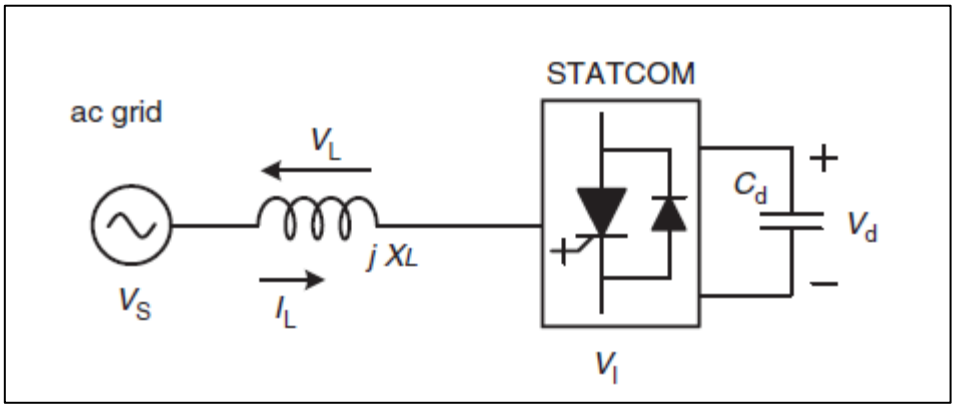

Figure 3-1 Simplified circuit for the ac grid and the D-STATCOM [26]

The D-STATCOM reactive power can be controlled if the magnitude of its V_I voltage is controlled, assuming that it is in phase with V_S so no real power is transferred [26].

- If V_S is equal to V_I, there is no reactive power and no active power in the D-STATCOM.
- · If V_S is larger than V_I, the D-STATCOM reactive power injection is inductive.
- · If V_S is smaller than V_I, the D-STATCOM reactive power injection is capacitive.

The operational characteristics of a D-STATCOM are shown in Figure 3-2.

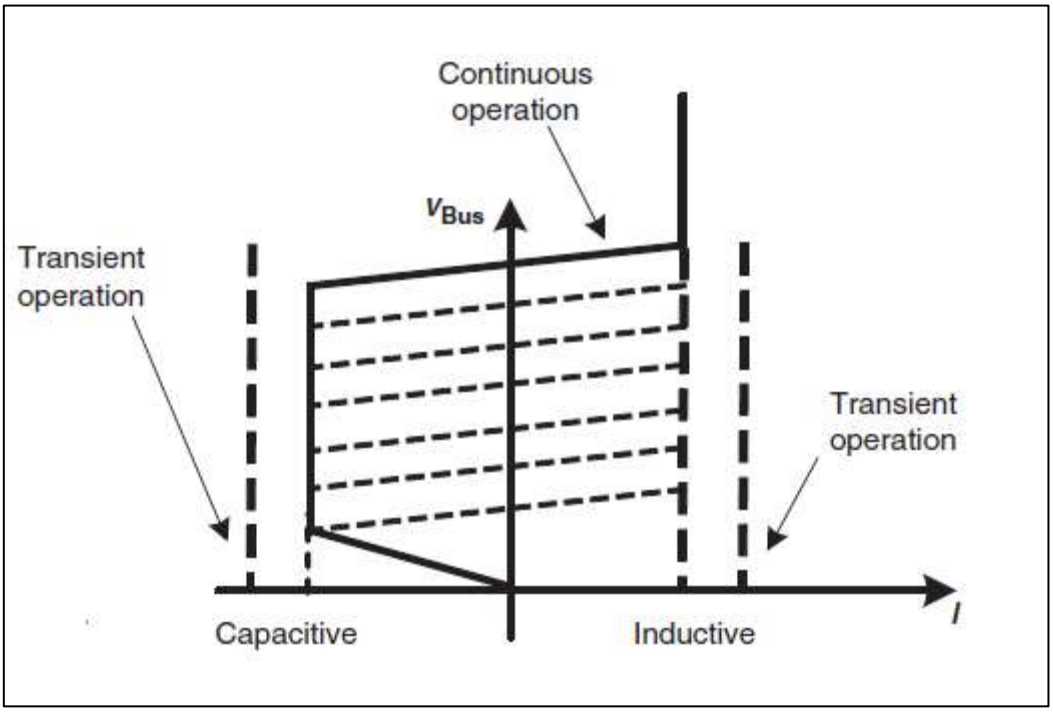

Figure 3-2 Operational characteristic of the D-STATCOM [26]

D-STATCOM operation allows continuous control of reactive power, but at a far higher speed through the use of PWM switching of IGBTs in the VSC [2].

3.1.4.2 Smart Inverters

Smart inverters are used as interfaced to connect the DC generation produced by the PV systems to the AC distribution systems. One of the capabilities, that distinguishes smart inverters is the ability to participate in Volt-var regulation. The Volt-var mode allows the inverter generate or absorb VARs based on the system voltage measured at the inverter terminals. By setting the parameters V1, V2, V3, V4, Q1, Q2, Q3, and Q4 shown at Figure 3-3, the inverter will determine the generation or absorption of VARs in the point of the interconnection with the distribution network [27].

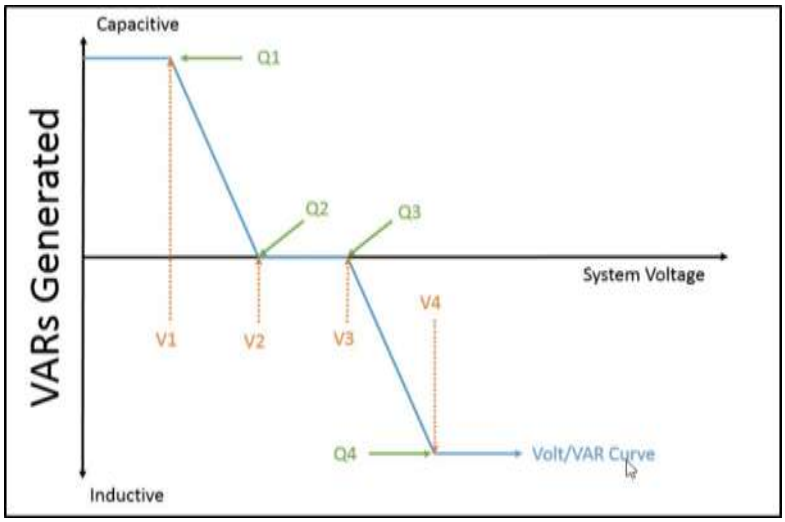

Figure 3-3 Volt-var curve of the smart inverter [27]

For this thesis the Volt-var characteristic of the smart inverters model in GridLAB-D will be using to simulate the operational characteristic of the D-STATCOM indicated in Figure 3-2.

3.2 SIZING AND LOCATION OF D-STATCOM USING A YBUS APPROACH

3.2.1 Network Equations

Circuit analysis using of the bus admittance matrix allows user to calculate the voltages and currents of the system in response to nodal current injections, as shown in (3.1) [28]. In this work the Y_{BUS} modified for fault studies is used.

$$\begin{bmatrix} Y_{11} & Y_{12} & Y_{13} & \cdots & Y_{1N} \\ Y_{21} & Y_{22} & Y_{23} & \cdots & Y_{2N} \\ Y_{31} & Y_{32} & Y_{33} & \cdots & Y_{3N} \\ \cdots & \cdots & \cdots & \cdots & \cdots \\ Y_{N1} & Y_{N2} & Y_{N3} & \cdots & Y_{NN} \end{bmatrix} \begin{bmatrix} V_{10} \\ V_{20} \\ V_{30} \\ \cdots \\ V_{N0} \end{bmatrix} = \begin{bmatrix} I_1 \\ I_2 \\ I_3 \\ \cdots \\ I_N \end{bmatrix} \tag{3.1}$$

Using matrix notation this can be expressed as:

$$YV=I \tag{3.2}$$

Where:

Y= the NxN bus admittance matrix.

V= the column vector of N bus voltages.

I= the column vector of N current injections.

The elements of the bus admittance matrix are classified into two types:

1) The diagonal elements (Y_{kk}), also called “self-admittance” of bus “k”, which are calculated as the sum of the admittances connected to bus “k” which includes sources, transformers, equivalent load impedances and line impedances.

2) The off-diagonal elements (Y_{kn}) for $k \neq n$, also called “mutual admittances”, which are the negative sum of admittances connected between buses “k” and “n”.

Since $Y_{kn} = Y_{nk}$ for most apparatus, the matrix Y will usually be symmetric [28].

3.2.2 Proposed Methodology

3.2.2.1 D-STATCOM Location and Sizing Criterion

The D-STATCOM placement will be determined by computing the voltage sensitivities due to current injections using the impedance matrix of the system (Z_{BUS}). The Z_{BUS} will be obtained from the inverse of the bus admittance matrix (Y_{BUS}).

By using the Z_{BUS} matrix and injecting capacitive currents into the different buses, two significant pieces information might be obtained about the system.

The first item is identifying which buses produce a higher ΔV when a capacitive current is injected, and the second point is the ability to compute the MVARs required by the system to obtain the desired voltages in each of the buses to meet the Range A or B levels established by the ANSI C84.1, depending on the study case.

3.2.2.3 Steps to Reactive Power Compensation

The proposed methodology to compensate reactive power in the system is comprised of the following steps:

Step 1: Read the distribution data (lines, buses, loads, generators).

Step 2: Perform the load flow by using the GridLAB-D program to compute the voltages for all the buses and the power losses in the system. Extract the Ybus matrix from GridLAB-D or build it manually based on the configuration of the system.

Step 3: Inject capacitive currents into each bus to evaluate which buses produce a higher incremental voltage (ΔV) in the system. These buses will be the potential candidates to locate the D-STATCOM in the power grid.

Step 4: Identify the critical voltage point in the system. Once the weakest point in the system is identified, evaluate the voltage levels for the other buses for that condition.

Step 5: Calculate the incremental voltage (ΔV) required to increase all the voltage magnitudes to the desired values (Range A or B).

Step 6: Try different capacitive currents until the desired ΔV is reached for all of the buses. Once the value of the D-STATCOM current to achieve this condition is determined; calculate the MVARs required.

Step 7: Run the power flow considering the reactive power compensation to calculate the new voltages and losses in the system.

3.3 RESILIENCE AND VOLTAGE STABILITY

The level of resilience of the power system measures the ability to stay stable in the face of a large transient event [17].

Voltage stability refers to the ability of a power system to maintain steady voltages at all buses in the system after being subjected to a disturbance from a given initial operating condition. It depends on the ability to maintain/restore equilibrium between load demand and power supply from the power system [29]. Figure 3-4 shows the classification of types of power system stability analysis.

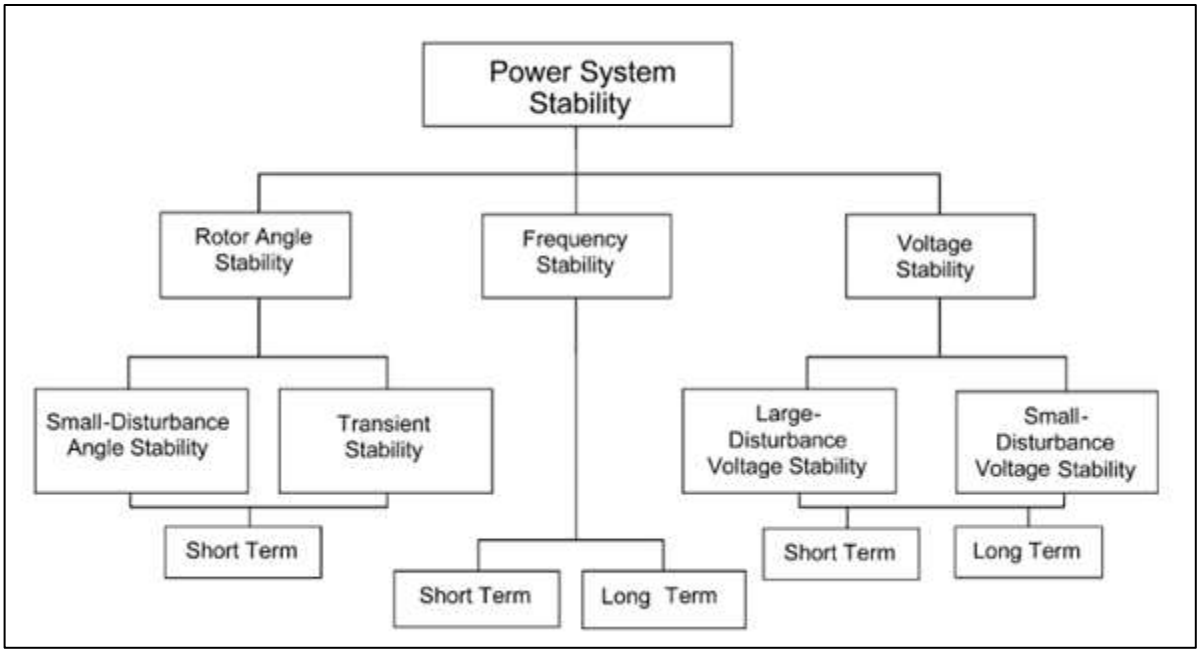

Figure 3-4 Classification of power system stability [29]

Small-disturbance voltage stability refers to the system's ability to maintain steady voltages when subjected to small perturbations such as incremental changes in system load. This form of stability is influenced by the characteristics of loads, continuous controls, and discrete controls at a given instant of time. This concept is useful in determining, at any instant, how the system voltages will respond to small system changes [29].

Voltage collapse is the process by which the sequence of events accompanying voltage instability leads to a blackout or abnormally low voltages in a significant part of the power system [29]. Generally, for transmission systems this is due to large events as triggers.

However, voltage stability limits for an electrical distribution network represent the maximum real or reactive load that can be placed at a given node in the system before voltage at that bus collapses [15].

D-STATCOM units can offer the ability to provide very fast dynamic Var injection, so their allocation in the power network could alleviate voltage instability or even prevent

voltage collapse [4]. QV curves for MDS modeled in GridLAB-D were developed in this project. The idea was to increase the reactive load for a given node and obtain the voltage values and in this way to determine the voltage stability limit with and without reactive power compensation. These curves will show how a prosumer voltage stability limit is increased with the addition of VARs into the system from D-STATCOMs. In this way the system becomes more resilient.

3.3 SCENARIOS TO STUDY

The studies in this work will target the residential test system. The residential test system is mainly radial with a main feeder coming from the distribution substation into the residential area which is divided mainly into 2 branches. Figure 3-5 shows the normal operating condition for the residential system. In this case, switches B2, B3 and B24 are open so, there will be two branches that feed the whole load (configuration 1). There is another system configuration shown in the Figure 3-6, that simulates an abnormal operational condition where it is necessary to feed the whole load using a common feeder. This condition is simulated by opening switch B4 and closing switch B2 (configuration 2). For the system shown in the Figure 3-5, there are different options to simulate contingency scenarios by varying the switch positions. However, for this study, the two different configurations mentioned previously will be simulated using GridLAB-D.

Figures 3-5 and 3-6 do not include a SVR in the branch between nodes 13 and 15. However, one of the cases to study will include it. Two cases will be simulated with and without D-STATCOMs:

- Case A: System without SVR applied to configuration 1 and 2.
- Case B: System with SVR applied to configuration 1.

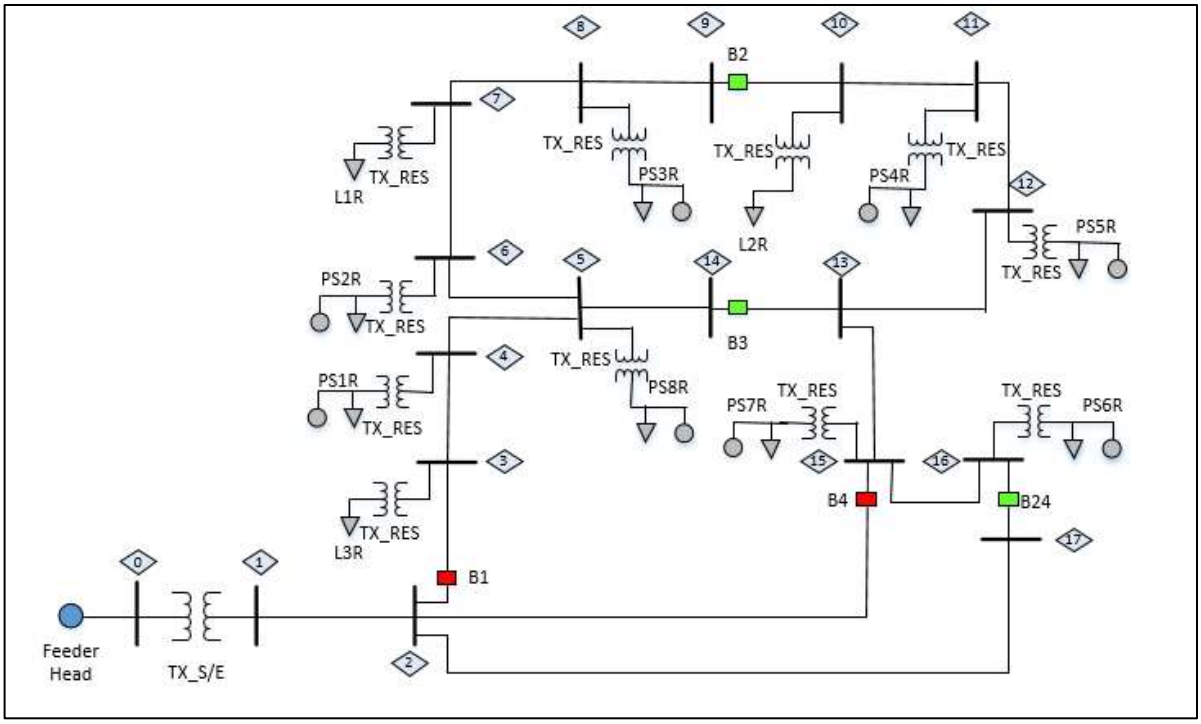

Figure 3-1 Residential EU during normal conditions of operation (configuration 1)

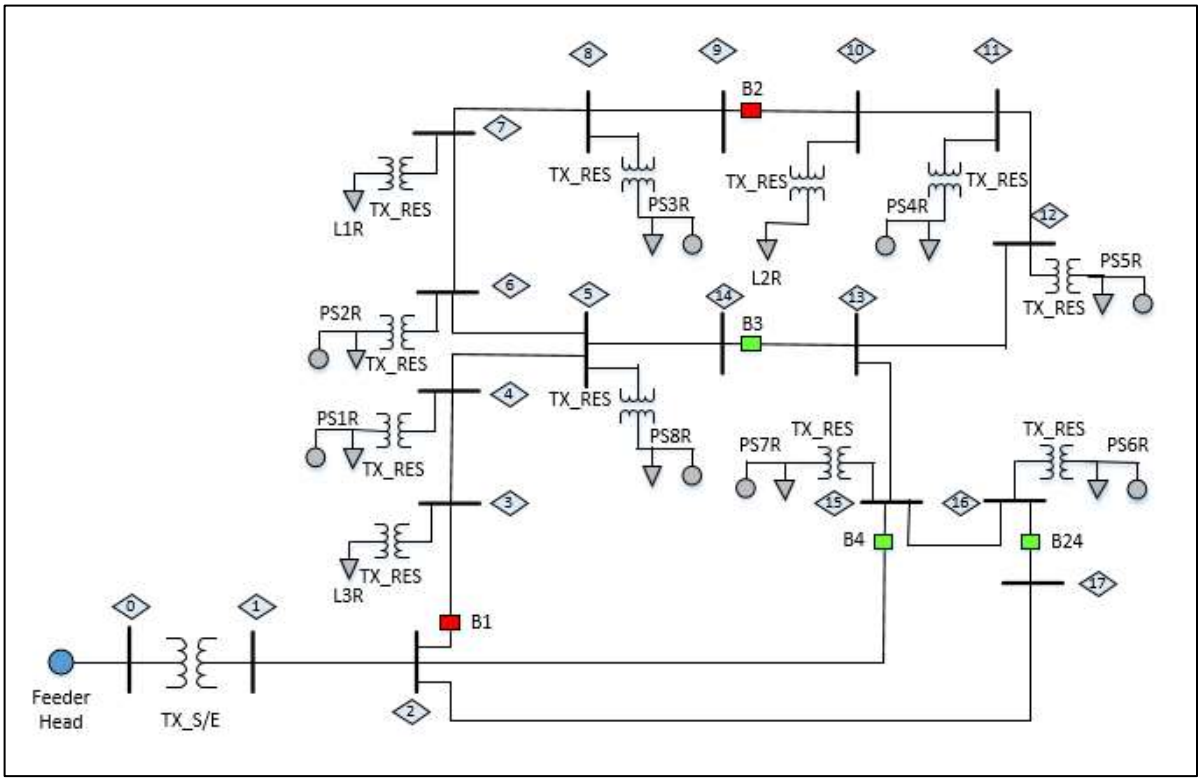

Figure 3-2 Residential EU during abnormal conditions of operation (configuration 2)

CHAPTER 4. SIMULATION RESULTS AND ANALYSIS

This study is comprised of numerous simulations based on the residential economic unit model. The results of several cases will be analyzed and discussed in this chapter.

4.2 SYSTEM ANALYSIS OVERVIEW

The MDS modeled for this study represents a residential distribution system characterized by a radial topology for the two main configurations to be analyzed as described in Section 3.3. Power will be provided from distribution substation connected to the bulk power system and from individual solar arrays belonging to prosumers connected to the feeders.

In general, the solar generation will be not enough to feed the loads of prosumers, let alone the rest of the feeder, therefore; electrical power from outside generation will be provide continuously in the system. Figure 4 –1 illustrates the behavior of the load and generation resources in the system for the date 2009-07-12 which is an example with high load consumption at 18:00:00 PDT during the summer season a time of the day when PV output is decreasing. This information was produced using the GridLAB-D residential load player based on a load dataset for the year 2009.

4.2 REACTIVE POWER COMPENSATION

The first step before to regulate the voltage in the system is to identify the critical voltages in the system. For configuration 1, which has two independent radial feeders, the buses with lower voltages in each branch will be identified. In the case of the configuration 2, the bus at the end of the main feeder will be the critical bus.

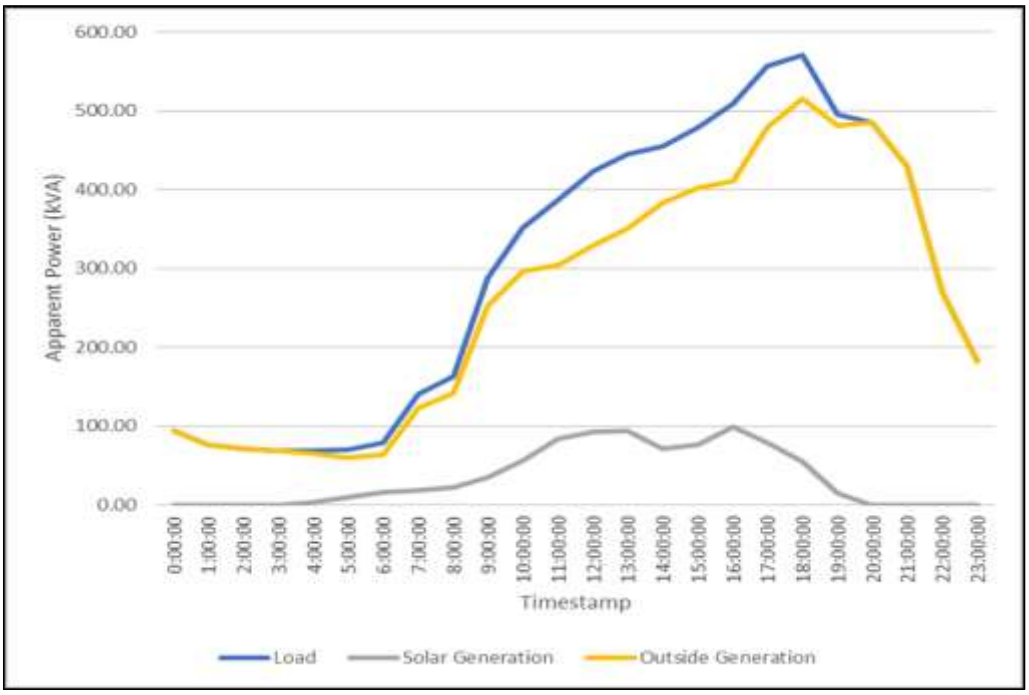

Figure 4-1 Load and generation behavior for the date 2009-07-12

The lower voltage limits established by ANSI C84.1 in Range A and Range B are 0.975 pu and 0.95 pu respectively. Configuration 1 represents a normal condition scenario, therefore; the minimum acceptable steady state voltage will be 0.975 pu. Configuration 2 represents an abnormal operational condition, so the minimum acceptable steady state voltage will be 0.95 pu. The maximum voltages allowed by the standard are very similar for both ranges and therefore; the value of 1.05 pu will be used in this study.

From Table 4-1 for configuration 1, the critical voltages are located at buses 8 and 9 on branch 1 and bus 10 on branch 2.

4.2.1 Case A: Compensation of the system without SVR

Table 4-1 contains the minimal voltages calculated for configuration 1 without any compensation in the system.

By applying the ZBUS approach described on Chapter 3, Table 4-1 indicates the incremental values of voltages desired at each bus to reach the minimum value of 0.975.

Table 4-1 Minimum Voltages at the Buses Configuration 1 without SVR

Bus Number	Minimum Voltages for Base Case	$\Delta V_{REQUIRED}$ for 0.975 pu
1	0.9994	-0.0244
2	0.9722	0.0028
3	0.9705	0.0045
4	0.9677	0.0073
5	0.966	0.009
6	0.9653	0.0097
7	0.9636	0.0114
8	0.9634	0.0116
9	0.9634	0.0116
14	0.966	0.009
10	0.9511	0.0239
11	0.9523	0.0227
12	0.958	0.017
13	0.9648	0.0102
15	0.9651	0.0099
16	0.9647	0.0103
17	0.9722	0.0028

The first step is to inject a unique capacitive current at each bus in the system, to identify which buses produce the highest ΔV. These buses will be considered as potential candidates to locate the D-STATCOM.

Table 4-2 Candidate buses to locate D-STATCOM on Branch 1 (Case A)

Bus Number	ΔV
9	0.03666
14	0.03719

Table 4-3 Candidate buses to locate D-STATCOM on Branch 2 (Case A)

Bus Number	ΔV
10	0.03484
11	0.02973

Table 4-2 and Table 4-3 show the largest voltage incremental values in pu obtained by injecting the same capacitive current (0.3i pu) at these buses. However, since the D-STATCOM will benefit the adjacent buses; it will not be enough to reach the $\Delta V_{REQUIRED}$ for the bus where the D-STATCOM will be located, but also the injection that allows all of the buses to reach 0.975. The capacitive current needs to be increased at the candidate buses shown in Table 4-2 and Table 4-3 to meet these conditions.

Since the topology in this case is radial, a more centric location for the compensation will be more beneficial, resulting in a D-STATCOM located at Bus 9, which also improves the voltage profiles for configuration 2. First, the D-STATCOM will be located at branch 1 and the voltage profile will be analyzed, and then the possible addition of a second D-STATCOM on branch 2 will be studied.

Once the location of the D-STATCOM is decided, the MVARs injections will be calculated. Incremental values of capacitive current were tested using Mathcad calculations until the $\Delta V_{REQUIRED}$ for all buses was met as indicated in Table 4-4.

The first and second columns in Table 4-4 show the Bus number and the voltage magnitudes from the solution with the minimum voltages over the course of the simulated year. The third column in Table 4-4 shows the change in voltage required at each bus to meet the Range A minimum values starting from the results in column 2.

The fourth column shows the minimum voltage obtained with GridLAB-D with the D-STATCOM in operations and the fifth column shows the change in voltage calculated in Mathcad using the Zbus method injecting the capacitive current in the Bus 9. The sixth column lists the change in voltage between the GridLAB-D results with and without the D-STATCOM (the difference between columns 4 and 2). The last column is the error between the results the change in voltage calculated with the Zbus approach and the change in voltage observed in GridLAB-D.

Table 4-4 Calculated Solution for D-STATCOM at Bus 9 on Branch 1 (Case A)

Bus Number	Minimum Voltage Base Case	$\Delta V_{REQUIRED}$	Min Voltages with D-STATCOM Bus 9	$\Delta V_{CALCULATED}$	$\Delta V_{OBTAINED}$	Error
1	0.9994	-0.0244	0.9996	0.0084	0.0001	0.0083
2	0.9722	0.0028	0.9780	0.0084	0.0059	0.0025
3	0.9705	0.0045	0.9769	0.0089	0.0064	0.0025
4	0.9677	0.0073	0.9752	0.0106	0.0075	0.0031
5	0.9660	0.0090	0.9743	0.0123	0.0083	0.0040
6	0.9653	0.0097	0.9741	0.0135	0.0087	0.0047
7	0.9636	0.0114	0.9740	0.0191	0.0104	0.0087
8	0.9634	0.0116	0.9742	0.0213	0.0109	0.0104
9	0.9634	0.0116	0.9766	0.0367	0.0132	0.0234
10	0.9511	0.0239	0.9571	0.0021	0.0060	-0.0039
11	0.9523	0.0227	0.9582	0.0023	0.0060	-0.0037
12	0.9580	0.0170	0.9639	0.0036	0.0059	-0.0023
13	0.9648	0.0102	0.9707	0.0055	0.0059	-0.0004
14	0.9660	0.0090	0.9743	0.0123	0.0083	0.0040
15	0.9651	0.0099	0.9710	0.0056	0.0059	-0.0003
16	0.9647	0.0103	0.9706	0.0054	0.0059	-0.0005
17	0.9722	0.0028	0.9780	0.0084	0.0059	0.0025

One capacitive current injection of 0.3i pu will provide the adequate compensation for branch 1. The MVARs required was computed based on a voltage of 0.975 at the D-STATCOM point of interconnection with the distribution system. Table 4-5 shows the calculated solution in this case.

Table 4-5 Calculated Solution for D-STATCOM on Branch 1 (Case A)

Bus Number	Size (MVAR)
9	5.85

GridLAB-D simulation results with the D-STATCOM added produce the bus voltage magnitudes shown in Figure 4-2.

Buses 1 through 9 and bus 14 are located on branch 1. The voltages at the buses on branch 1 improved considerably and are very close to 0.975 pu. The Table 4-4 indicates the difference between the incremental values calculated in Mathcad by using the Z_{BUS} approach and the results of the simulation using GridLAB-D.

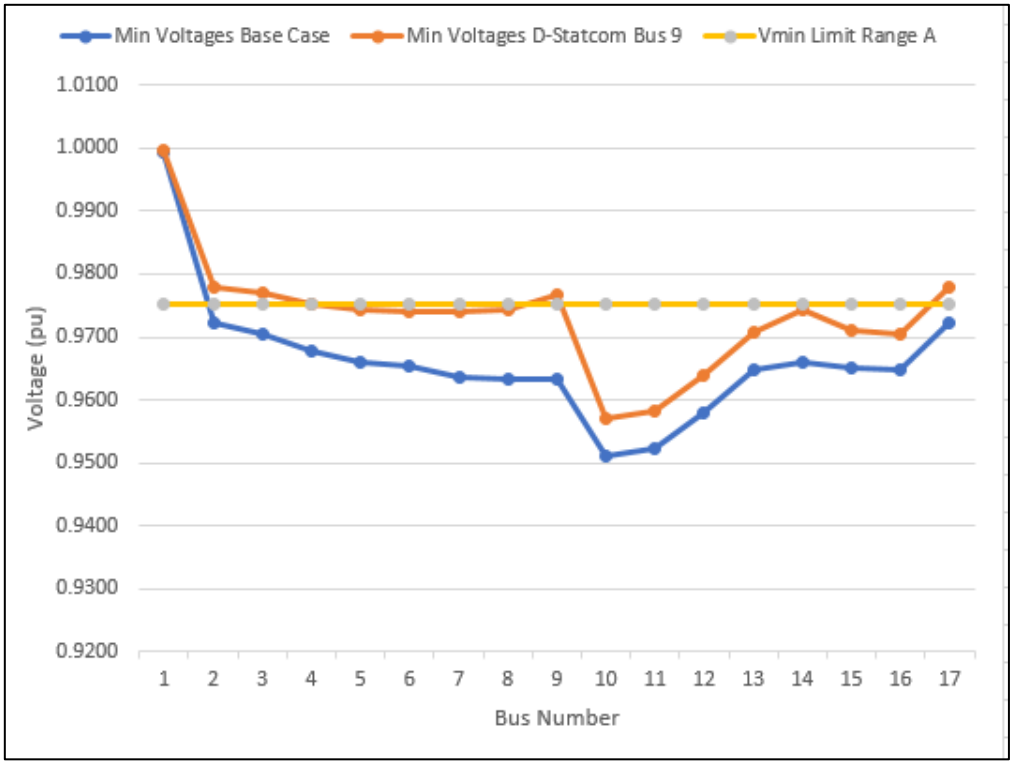

Figure 4-2 Minimum voltages profile with D-STATCOM at Bus 9 (Case A)

The D-STATCOM placed at Bus 9 does not provide much compensation for branch 2, so buses 10-13 and 15-17 show less improvement. Therefore, a second D-STATCOM will

be located on branch 2. The goal is to reach the $\Delta V_{REQUIRED}$ for buses 10,11 and 12. The same procedure is applied by using the Z_{BUS} and injecting capacities currents to determine which one is the appropriate to compensate voltages at these buses. In this case a current of 0.33 pu, and 6.435 MVAR injected at bus 11 was needed, as shown in Table 4-6.

Table 4-6 Calculates Solution for D-STATCOM on Branch 2

Bus Number	Size (MVAR)
11	6.435

By running the GridLAB-D using the second D-STATCOM, the results show the voltages decreased instead of increasing, as shown in Figure 4-3.

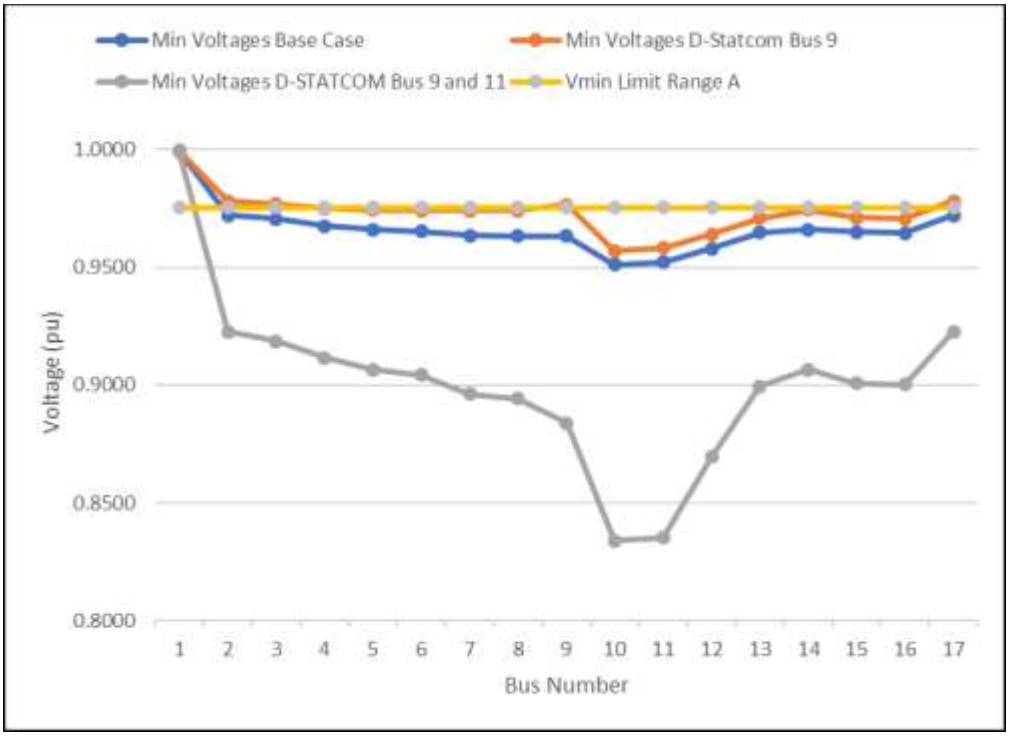

Figure 4-3 Minimum voltage profile with D-STATCOM at Bus 11

Further analysis showed that the two D-STATCOMs fought each other in the solution with one supplying Q and the other consuming in one interval and reversing in the next. Therefore, this solution is not affordable by using GridLAB-D with inverters controlled in

Volt-var regulation. An inverter in constant PQ mode will instead be installed at bus 11 to improve the voltage in this point with the other inverter is in Volt-var regulation.

Since the calculation in Table 4-6 did not include the D-STATCOM at Bus 9, a D-STATCOM with a rating less than that value were tested in GridLAB-D. With 2.145 MVAR injected at bus 11, the minimum point in the voltage profile reached a 0.97 pu value, which is still below the minimum for Range A. It will be necessary to increase the injection of reactive power at Bus 11. By testing different values into GridLAB-D, it was determined that 2.85 MVAR as shown in Table 4-7 was the adequate to reach a minimum voltage of 0.975 pu. Figure 4-4 shows the new voltage profile.

Table 4-7 Tested Solution for PQ Inverter on Branch 2

Bus Number	Size (MVAR)
11	2.85

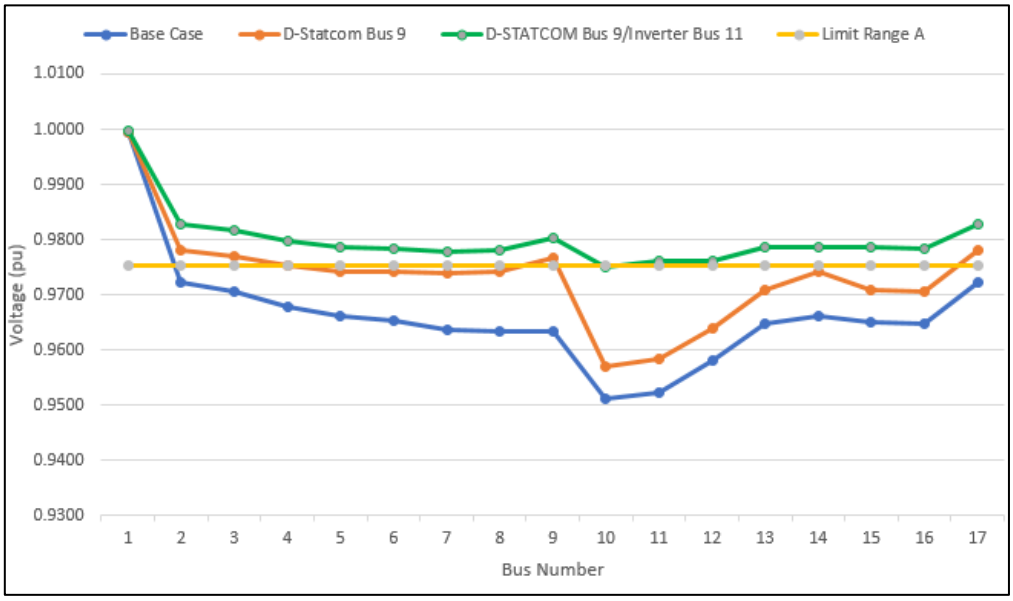

Figure 4-4 Minimum Voltage with Volt-var controlled D-STATCOM at Bus 9 and, constant PQ D-STATCOM at Bus 11

Figure 4-5 illustrates the maximum voltages at each bus in the system for 2009 year. None exceed the upper limit established by the Standard ANSI C84.1 under normal operating conditions. During low load demand in the system, the voltages will reach its maximum value. Figure 4-5 shows the maximum voltages obtained without compensation (base case), with a Volt-var controlled D-STATCOM connected at Bus 9 only and, with Volt-var controlled D-STATCOM connected at Bus 9 plus a constant PQ D-STATCOM at Bus 11. When both D-STATCOMs are working in the system, the branch 2 tends to have higher maximum voltages because of the constant Q injection at bus 11 which is independent of the voltage measured at the terminals of this D-STATCOM.

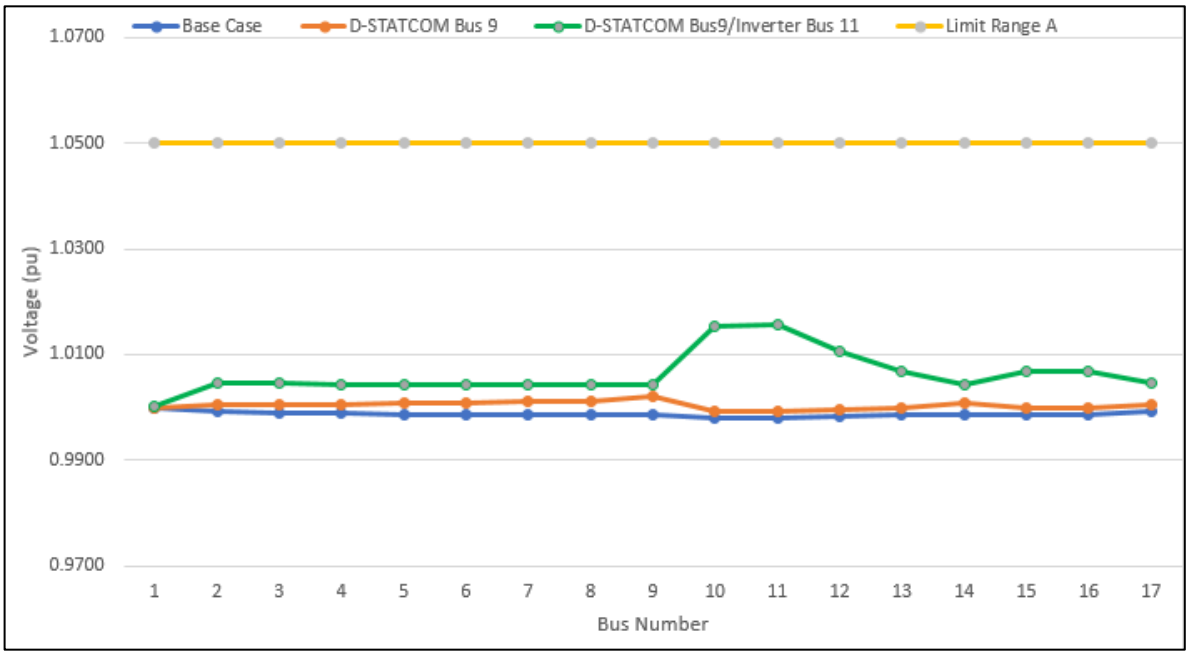

Figure 4-5 Maximum Voltage with Volt-var controlled D-STATCOM at Bus 9 and, constant PQ D-STATCOM at Bus 11

Once the level of compensation has been defined for the system under normal operating conditions, the next step will be to determine if reactive compensation made for configuration 1 also works properly for configuration 2, which requires a minimum voltage at the buses of 0.95 pu. Figures 4-6 and 4-7 show the minimum and maximum voltages for

the configuration 2 with D-STATCOMs rated as calculated for configuration 1. The Range B for the ANSI C84.1 are not exceeded for this scenario.

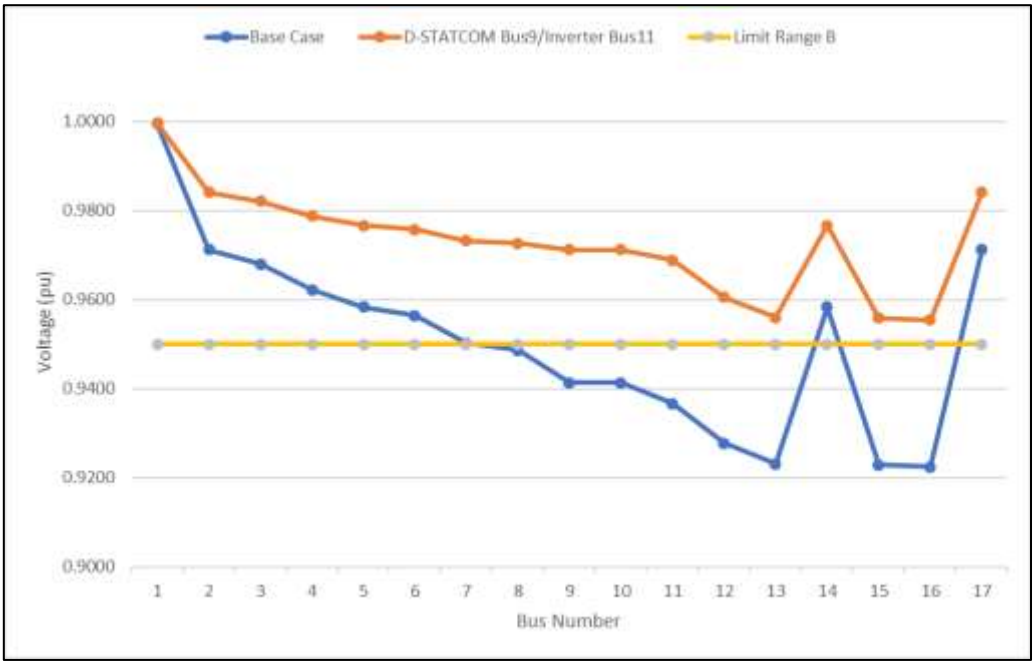

Figure 4-6 Minimum Voltage with Volt-var controlled D-STATCOM at Bus 9 and, constant PQ D-STATCOM at Bus 11 for Configuration 2

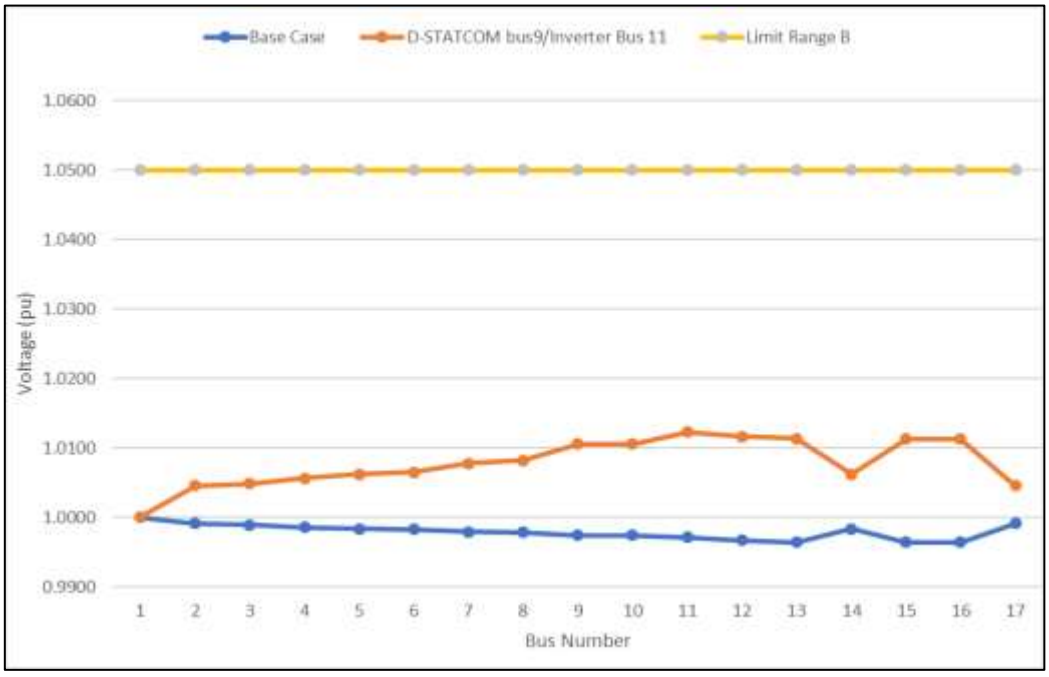

Figure 4-7 Maximum Voltage with Volt-var controlled D-STATCOM at Bus 9 and, constant PQ D-STATCOM at Bus 11 for Configuration 2

4.2.1.1 Reduction of System Losses

Since the injection of reactive power in the system is in a way local, it should also impact system losses. Table 4-8 shows the maximum real and reactive losses with and without the reactive power compensation.

Table 4-8 Maximum System Losses Case A

Configuration 1	Base Case	With D-STATCOMs	Losses Reduction
Real Power Losses (kW)	40.57	28.66	11.91
Reactive Power Losses (kVAR)	319.10	231.48	87.62

4.2.1.2 Reduction of Peak Demand

The reduction of peak demand in the system with and without the reactive power compensation is shown in Table 4-9.

Table 4-9 Maximum Peak Demand Case A

Configuration 1	Base Case	With D-STATCOMs	Peak Demand Reduction
Active Power (MW)	5.15	5.14	0.01
Reactive Power (MVAR)	4.29	2.52	1.77

4.2.2 Case B: Compensation of the system with SVR

Table 4-10 contains the minimal voltages calculated for configuration 1 without any compensation in the system and with a voltage regulator connected between buses 13 and 15. Even when GridLAB-D neglects the voltage regulator losses a small value of impedance might be used. For this work, an impedance of 0.0001+0.0001j was used in Mathcad to represent the voltage regulator impedance in the $Z_{BUS.}$

By applying the Z_{BUS} approach explained on Chapter 3, Table 4-10 indicates the incremental values of voltages desired for each bus to reach the minimum value of 0.975.

Table 4-10 Minimum Voltages at the Buses Configuration 1 with SVR

Bus Number	Minimum Voltages for Base Case	$\Delta V_{REQUIRED}$ for 0.975 pu
1	0.9994	-0.0244
2	0.9722	0.0028
3	0.9705	0.0045
4	0.9677	0.0073
5	0.9660	0.0090
6	0.9654	0.0096
7	0.9637	0.0113
8	0.9634	0.0116
9	0.9634	0.0116
10	0.9787	-0.0037
11	0.9792	-0.0042
12	0.9818	-0.0068
13	0.9848	-0.0098
14	0.9660	0.0090
15	0.9651	0.0099
16	0.9647	0.0103
17	0.9722	0.0028

Similar to the procedure applied for the case A, the first step was to inject a unique capacitive current to each bus in the system, to identify which buses produce the higher ΔV. These buses will be considered the potential candidates to locate the D-STATCOM.

Table 4-11 Candidate buses to locate D-STATCOM on Branch 1 (Case B)

Bus Number	ΔV
9	0.05131
14	0.05205

Table 4-12 Candidate buses to locate D-STATCOM on Branch 2 (Case B)

Bus Number	ΔV
10	0.04868
11	0.04149

Table 4-11 and Table 4-12 show up the largest voltage incremental values in pu obtained by injecting the same capacitive current (0.42i pu) at these buses. However, since the D-STATCOM will benefit the adjacent buses; it will not be enough to reach the $\Delta V_{REQUIRED}$ for the bus where the D-STATCOM will be located, but also the rating that allows all of the buses to reach at least 0.975. The capacitive current needs to be increased at the candidate buses shown in Table 4-11 and Table 4-12 to meet these conditions.

Since the topology in this case is radial, a more centric location of the compensation will be more beneficial. Choosing the bus 14 to place the D-STATCOM and using incremental values of capacitive current were tested using the Mathcad calculation until meet the $\Delta V_{REQUIRED}$ for all the buses, was met as indicated in Table 4-13.

The first and second columns in Table 4-13 show the Bus number and the voltage magnitudes from the solution with the minimum voltages over the course of the simulated year. The third column in Table 4-13 shows the change in voltage required at each bus to meet the Range A minimum values starting from the results in column 2.

The fourth column shows the minimum voltage obtained with GridLAB-D with the D-STATCOM in operations and the fifth column shows the change in voltage calculated in Mathcad using the Zbus method injecting the capacitive current in the Bus 14. The sixth column lists the change in voltage between the GridLAB-D results with and without the D-STATCOM (the difference between columns 4 and 2). The last column is the error between the results the change in voltage calculated with the Zbus approach and the change in voltage observed in GridLAB-D.

Table 4-13 Calculated Solution for D-STATCOM at Bus 14 on Branch 1 (Case B)

Bus Number	Minimum Voltage Base Case	$\Delta V_{REQUIRED}$	Min Voltages with D-STATCOM Bus 14	$\Delta V_{CALCULATED}$ - Bus14	$\Delta V_{OBTAINED}$ - Bus14	Error
1	0.9994	-0.0244	0.9992	0.0164	-0.0002	0.0166
2	0.9722	0.0028	0.9442	0.0164	-0.0280	0.0444
3	0.9705	0.0045	0.9396	0.0175	-0.0309	0.0484
4	0.9677	0.0073	0.9309	0.0207	-0.0368	0.0575
5	0.9660	0.0090	0.9249	0.0240	-0.0412	0.0652
6	0.9654	0.0096	0.9242	0.0226	-0.0412	0.0638
7	0.9637	0.0113	0.9225	0.0193	-0.0412	0.0605
8	0.9634	0.0116	0.9222	0.0188	-0.0412	0.0600
9	0.9634	0.0116	0.9222	0.0188	-0.0412	0.0600
10	0.9787	-0.0037	0.9216	0.0041	-0.0571	0.0612
11	0.9792	-0.0042	0.9226	0.0046	-0.0566	0.0612
12	0.9818	-0.0068	0.9276	0.0072	-0.0542	0.0614
13	0.9848	-0.0098	0.9335	0.0109	-0.0513	0.0622
14	0.9660	0.0090	0.9009	0.0570	-0.0652	0.1222
15	0.9651	0.0099	0.9371	0.0109	-0.0280	0.0390
16	0.9647	0.0103	0.9366	0.0105	-0.0281	0.0385
17	0.9722	0.0028	0.9442	0.0164	-0.0280	0.0444

One capacitive current injection of 0.46i pu will provide the adequate compensation to the system. The MVARs required was computed based on a voltage of 0.975 at the D-STATCOM point of interconnection with the distribution system. Table 4-14 shows the calculated solution in this case.

Table 4-14 First Calculated Solution for D-STATCOM on Branch 1 (Case B)

Bus Number	Size (MVAR)
14	8.97

The GridLAB-D results using a single D-STATCOM on bus 14, show that the voltages decreased instead of increasing, as shown in Figure 4-8. This again appears to be because the SVR and D-STATCOM are fighting each other.

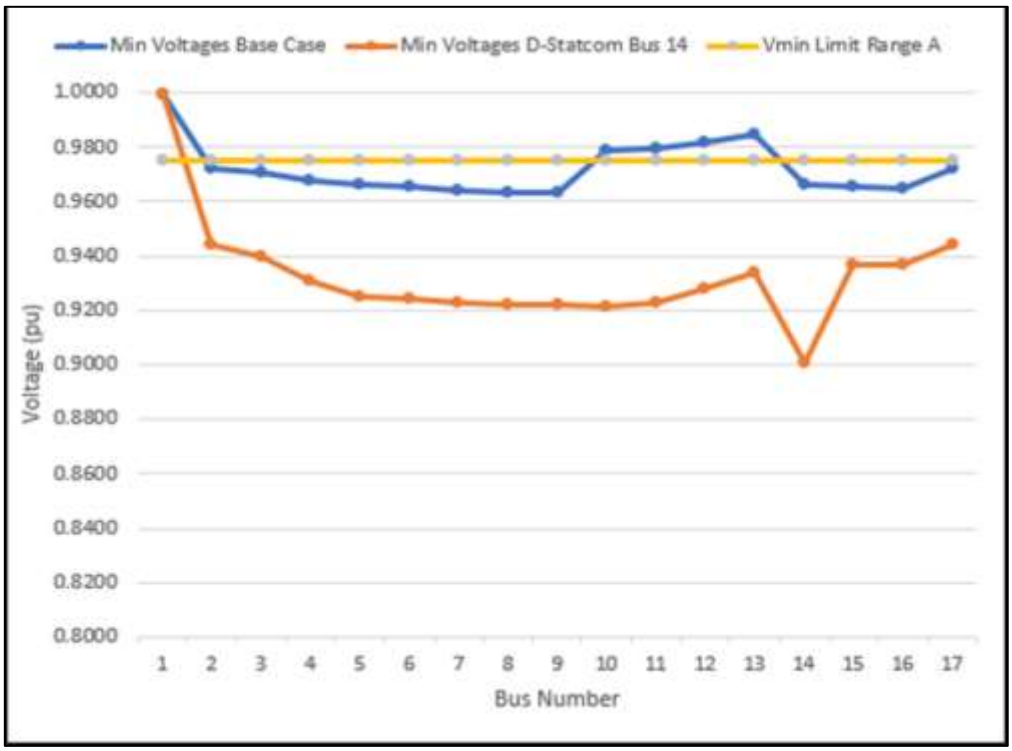

Figure 4-8 Minimum voltage profile with D-STATCOM at Bus 14 (Case B)

A second option to compensate the case B was to place a D-STATCOM in bus 9 which is the other candidate. In this case a higher current of 0.58i pu is needed to compensate the whole system to meet the $\Delta V_{REQUIRED}$ shown in Table 4-15. Table 4-16 shows the calculated solution in this case and compares to the GridLAB-D results.

Table 4-15 Calculated Solution for D-STATCOM at Bus 9 on Branch 1 (Case B)

Bus Number	Minimum Voltage Base Case	$\Delta V_{REQUIRED}$	Min Voltages with D-STATCOM Bus 9	$\Delta V_{CALCULATED}$ - Bus9	$\Delta V_{OBTAINED}$ - Bus9	Error
1	0.9994	-0.0244	0.9999	0.0162	0.0004	0.0158
2	0.9722	0.0028	0.9983	0.0162	0.0261	-0.0099
3	0.9705	0.0045	0.9983	0.0173	0.0278	-0.0105
4	0.9677	0.0073	0.9983	0.0204	0.0306	-0.0102
5	0.9660	0.0090	0.9985	0.0237	0.0324	-0.0087
6	0.9654	0.0096	0.9986	0.0260	0.0332	-0.0072
7	0.9637	0.0113	0.9991	0.0369	0.0355	0.0015
8	0.9634	0.0116	0.9993	0.0412	0.0359	0.0052
9	0.9634	0.0116	1.0008	0.0709	0.0374	0.0334
10	0.9787	-0.0037	0.9943	0.0041	0.0156	-0.0115
11	0.9792	-0.0042	0.9945	0.0046	0.0153	-0.0107
12	0.9818	-0.0068	0.9956	0.0071	0.0139	-0.0068
13	0.9848	-0.0098	0.9969	0.0108	0.0122	-0.0014
14	0.9660	0.0090	0.9985	0.0237	0.0324	-0.0087
15	0.9651	0.0099	0.9969	0.0108	0.0318	-0.0210
16	0.9647	0.0103	0.9969	0.0103	0.0322	-0.0218
17	0.9722	0.0028	0.9983	0.0162	0.0261	-0.0099

Table 4-16 Second Calculated Solution for D-STATCOM on Branch 1 (Case B)

Bus Number	Size (MVAR)
9	11.31

The results from GridLAB-D using a single D-STATCOM on bus 9 show that the minimum voltages of all of the buses exceed 0.975 pu, as shown in Figure 4-9. However, this solution also causes the maximum voltages of some of the buses to exceed 1.05 pu as it is shown at Figure 4-10. Therefore, the method applied by using Z_{BUS} in Mathcad does not match the results from GridLAB-D.

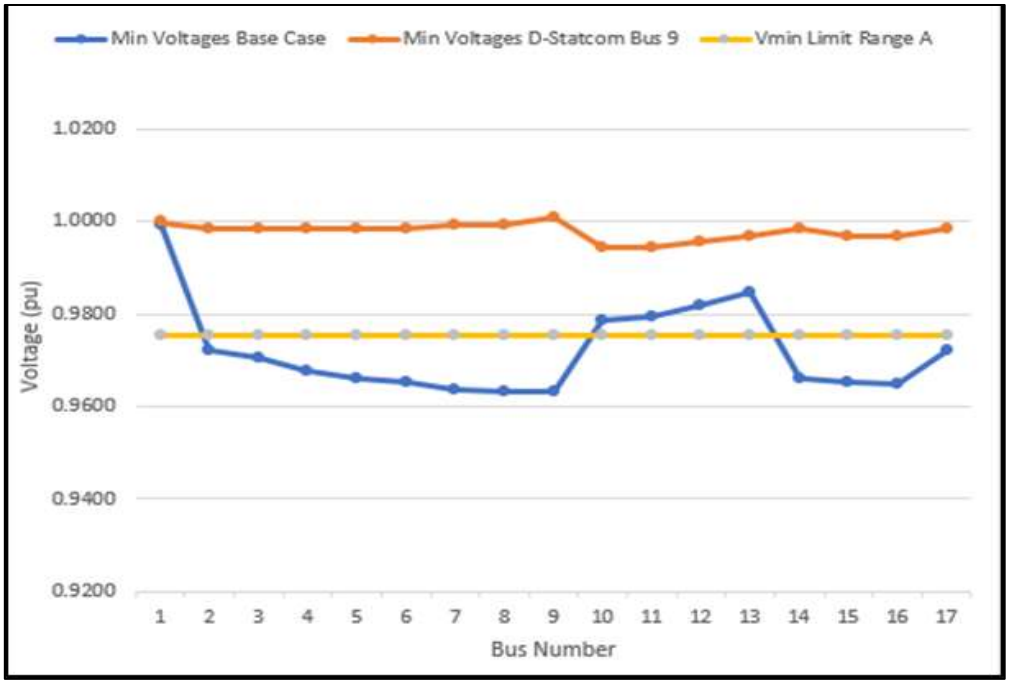

Figure 4-9 Minimum voltage profile with D-STATCOM at Bus 9 (Case B)

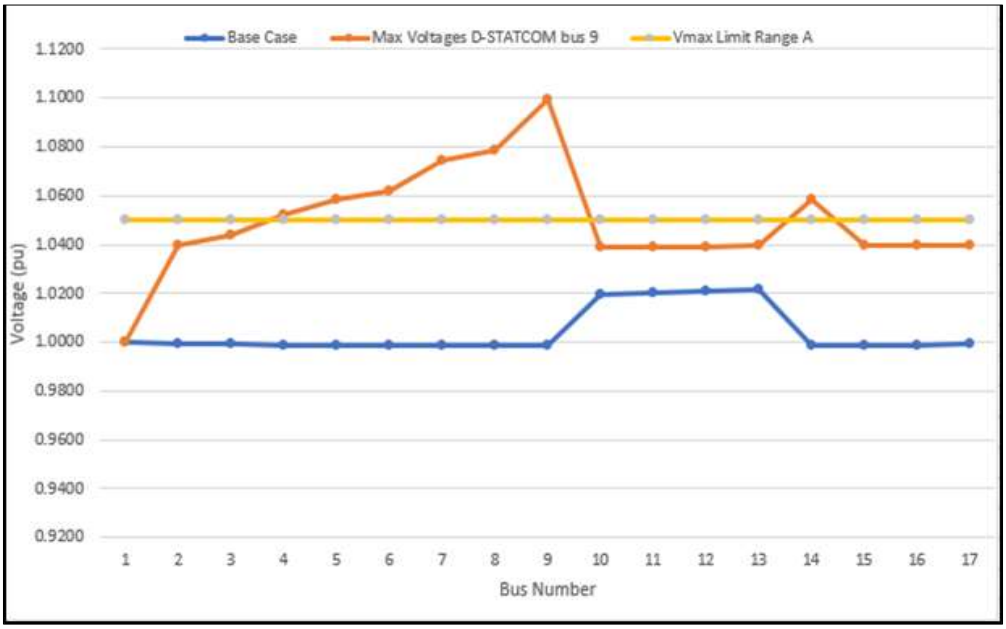

Figure 4-10 Maximum voltage profile with D-STATCOM at Bus 9 (Case B)

Since the compensation in Bus 9 was close to meet the requirements, different values of compensation were tested at other locations to find an approximate solution. This suggested placement of the D-STATCOM at bus 8. Table 4-17 shows the approximate solution for this case. The minimum and maximum voltages are shown in Figures 4-11 and 4-12. With this placement the voltage at buses 15 and 16 are very close to the minimum voltage value allowed, which is 0.975 pu.

Table 4-17 Final Approximate Solution for D-STATCOM on Branch 1 (Case B)

Bus Number	Size (MVAR)
8	7.22

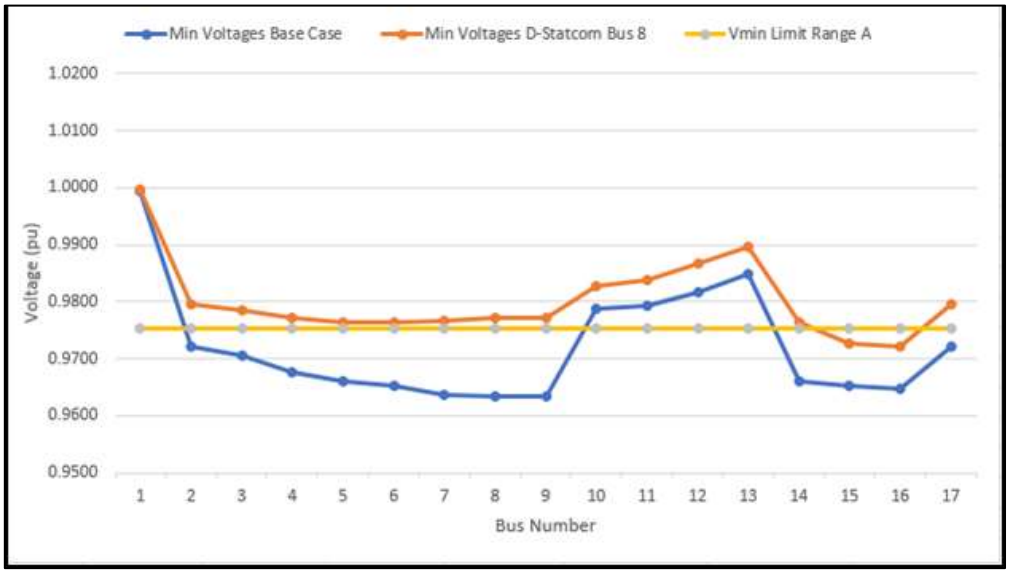

Figure 4-11 Minimum voltage profile with D-STATCOM at Bus 8 (Case B)

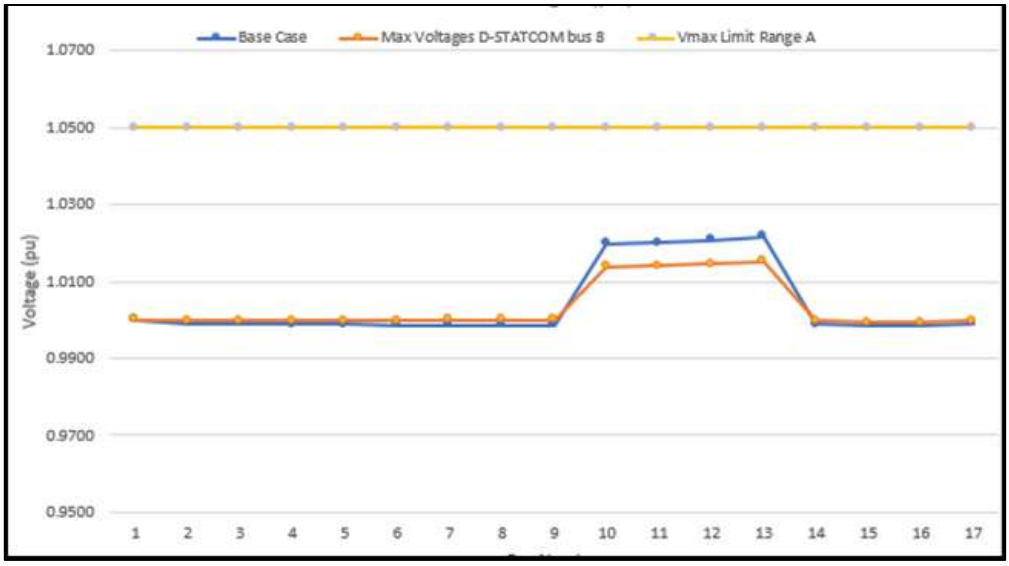

Figure 4-12 Maximum voltage profile with D-STATCOM at Bus 8 (Case B)

4.2.2.1 Reduction of System Losses

Table 4-18 shows the maximum real and reactive losses with and without the reactive power compensation.

Table 4-18 Maximum System Losses Case B

Configuration 1	Base Case	With D-STATCOM	Losses Reduction
Real Power Losses (kW)	39.98	31.96	8.02
Reactive Power Losses (kVAR)	316.76	259.51	57.25

4.2.2.2 Reduction of Peak Demand

The reduction of peak demand in the system with and without the reactive power compensation is shown in Table 4-19.

Table 4-19 Maximum Peak Demand Case B

Configuration 1	Base Case	With D-STATCOM	Peak Demand Reduction
Active Power (MW)	5.15	5.14	0.01
Reactive Power (MVAR)	4.29	3.10	1.19

4.2.3 Results

4.2.3.1 Case A

The results from computations and simulations for case A were the following:

- The incremental voltage values calculated in Mathcad with the Z_{BUS} that was built manually were different than those obtained with the use of the GridLAB-D. This can be observed in the last column of the Table 4-4, which corresponds to the error between the results from GridLAB-D and Mathcad. For branch 1 the GridLAB-D values were smaller than those calculated in Mathcad. The higher errors were for the buses 7, 8 and 9. For branch 2, the result was the opposite since the $\Delta V_{OBTAINED}$ were higher than those calculated in Mathcad except for the bus 17. Therefore, negative errors were obtained. However, even when the $\Delta V_{OBTAINED}$ were higher than those calculated in Mathcad, the voltages did not reach totally 0.975 pu.
- With the incorporation of a second D-STATCOM on branch 2, the voltage magnitudes from GridLAB-D went down rather to increase. Therefore, a problem of Volt-var control in the model was found when there was more than one inverter operating under the Volt-var mode in the same simulation case.

- To reach an adequate level of compensation, the mode of the second D-STATCOM located on branch 2 was changed to constant PQ, and by testing different values of MVA injections; a minimum voltage of 0.975 was obtained for the voltage profile.
- The solution with D-STATCOM in Volt-var control at Bus 9 and a D-STATCOM in constant PQ D-STATCOM at bus 11 was later tested in the configuration 2 of the system and it was demonstrated that the compensation meets the Range B of the ANSI C84.1.
- A reduction for system real and reactive losses and peak demand on the system were observed in the results obtained as expected.

4.2.3.2 Case B

The results from computations and simulations for case B were the following:

- The incremental voltage values calculated in Mathcad with the Z_{BUS} that was built manually were different than those obtained with the use of the GridLAB-D. All of $\Delta V_{OBTAINED}$ were negative, which indicates that the voltage in the buses decreased instead to increase with the D-STATCOM added at Bus 14.
- The Z_{BUS} method does not correctly predict the required MVARs to be injected in the system, instead; the MVARs can be used as a reference to run different power flow simulations in GridLAB-D to obtain an acceptable solution.
- A reduction for losses and peak demand on the system were observed in the results obtained. In this case, the reduction for losses were less because of the slightly less Q injection locally compared with Case A.

4.5 RESILIENCE IMPROVEMENT

4.5.1 Voltage Stability

A resilient system is able to stay stable in the face of a large transient event [17]. By injecting reactive power at key locations in distribution systems, the system will be able to withstand larger disturbances or abnormal operating conditions. One of the effects of the reactive power compensation is to extend the voltage stability limits for the system. Figure 4-13 shows how the voltage stability limit for the prosumer PS3R (bus 8) is extended by comparing the voltage stability limit of the system without D-STATCOM and with D-STATCOM in the system.

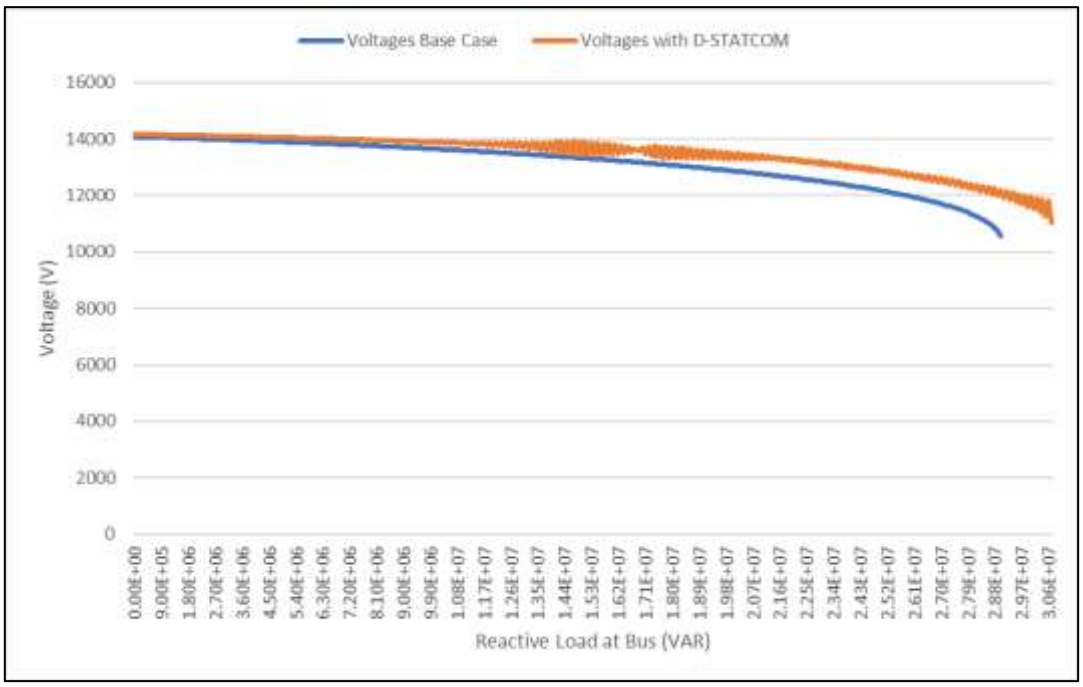

Figure 4-13 Impact of the reactive power compensation on voltage stability limits in bus 8

Figure 4-13 shows that the bus 8 can be loaded with a higher reactive load before voltage at that bus collapses, therefore; a resilient metric related the amount of compensation,

and the new voltage stability limits could provide a very general idea about how the reactive compensation improves the resilience of the distribution systems.

CHAPTER 5. TESTING SOLAR POWER SYSTEM FOR STAND-ALONE APPLICATIONS

5.1 INTRODUCTION

The results shown in this chapter represent the measurements from two different types of PV panels available for a small stand-alone lighting application. The main goal of this project is to implement lighting devices that are controlled wirelessly by a controller. Since the devices are not connected to a power supply, these are considered stand-alone devices which will generate their own power using solar cell installed in the package plus a battery system to provide the energy during the night.

5.2 TESTING GOALS

- Determine the Maximum Power Point (MPP) for the PV small systems during different seasons (Fall, Winter and Spring).
- Measure the solar irradiation available during the tests.
- Generate the V-I characteristic for each PV system.
- Determine the efficiency of each PV system to determine if they are adequate for this application.

5.3 THEORY BEHIND PHOTOVOLTAIC SOLAR ENERGY

5.3.1 Photovoltaic System

A material or device which converts sunlight into some voltage and current referred to as photovoltaic (PV). Semiconductor materials have been used as photovoltaic devices to convert sunlight into electricity. A solar PV cell is the most basic device in a PV system. Arrays and modules are obtained by grouping the PV cells to obtain different ranges of voltages and currents. Small applications of PV systems can feed small loads such as lighting systems or

DC Motors with simple electronic interfaces. When more developed applications with higher ratings or more complicated power needs are required, power electronic converters are implemented to regulate the voltage and the current to the load, to control the power flow in grid-connected systems and to track the maximum power point (MPP) of the PV device [30].

5.3.2 How a PV Cell Works

A photovoltaic cell is a semiconductor diode that conducts when exposed to the light. The semiconductor material in most commercial PV cells are the monocrystalline or polycrystalline Silicon. For the case of Silicon cells, these are comprised of a thin layer of bulk Si or a thin Si film connected to electrical terminals. To create the p-n junction one portion of the Si layer should be doped. A thin metallic grid is placed at the sun-facing surface. Figure 5-1 shows the physical structure of a PV cell [30].

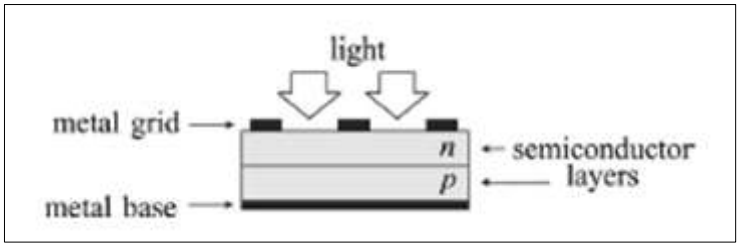

Figure 5-1 Physical structure of a PV cell [30]

The solar radiation is composed of photons which have an associated level of energy. When the sunlight strikes the PV cell surface, the cell produces charge carriers that will generate an electrical current when the terminals of the PV are short-circuited or some load is connected.

The energy obtained from the incident photon is enough to detach the covalent electrons of the semiconductor. This depend on the semiconductor material and on the wavelength of the incident light.

The capacity of absorption of a semiconductor depends on many factors such as the semiconductor bandgap, the reflectance of its surface, on the inherent concentration of carriers of the semiconductor, on the recombination rate and on the temperature [30].

The band-gap energy (Eg) is the energy that the electrons in the semiconductor material must acquire to jump towards the conduction band. The units for the band-gap energy are electron-volts (eV).

The band-gap for Silicon is 1.12 eV, which is the energy required by the electron to free itself from the electrostatic force that bonds it to the nucleus [31]. When a photon with more than 1.12 eV of energy is absorbed by a solar cell, a single electron may jump to the conduction band. Therefore, photons with energies lower than the band-gap of the PV cell do not produce any voltage or current. Photons with energy values higher than 1.12 eV can produce electricity, but only the band-gap energy is used for voltage, the rest of the energy is dissipated as heat in the PV cell [30]. In the case of the Silicon PV cells, photons with wavelengths greater than 1.11 μm have energy, *hv,* less than the 1.12-eV band-gap energy needed to excite an electron, and photons with wavelength shorter than 1.11 μm have the enough energy to excite an electron. The Figure 5-2 indicates the usable energy for a Silicon PV cell [31].

5.3.3 Solar Spectrum

The efficiency of a PV cell depends on the solar radiation spectrum. The sun is considered as a light source whose radiation spectrum may be compared to the spectrum of a black body near 6000 K which absorbs or emits electromagnetic waves that covers the whole range of wavelengths. Since the spectrum of the sunlight reaching the Earth's surface is

affected by factors such as: temperature on the solar disc location and on the influence of the atmosphere, the studies related to PV devices performance have been complicated [31].

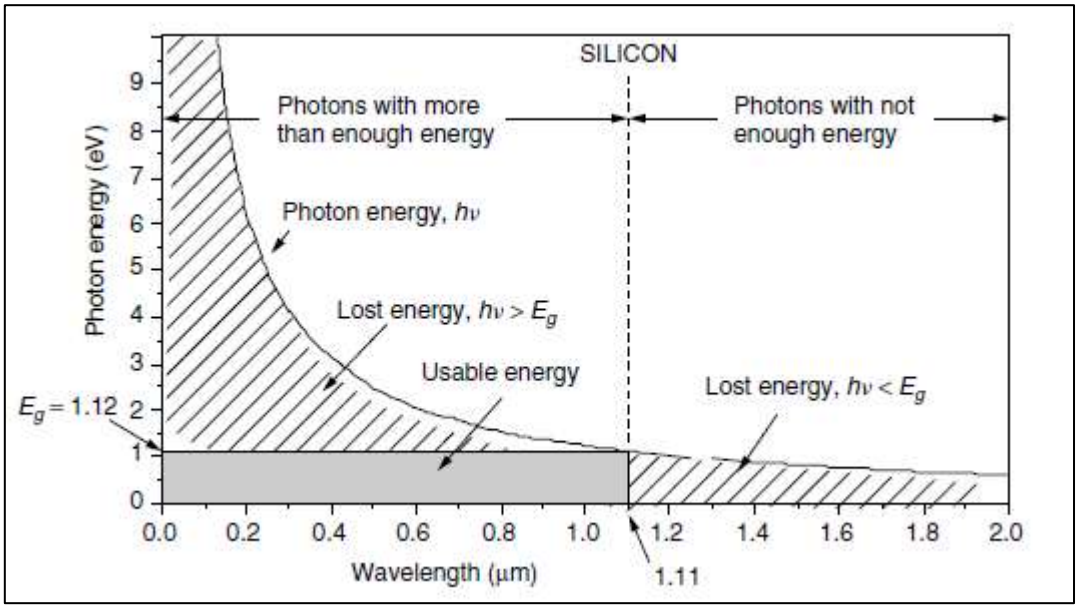

Figure 5-2 Usable energy for silicon PV cell [31]

In extraterrestrial space, the solar radiation has been estimated to a value of 1.353 kW/m^2. On the Earth's surface, the solar radiation is assumed to be approximately 1 kW/m^2, which is only a reference value due to all the factors that can cause variations in this value.

The air mass (AM) is defined as the mass of air that exists between the Earth's surface and the sun which is responsible of the spectral distribution and intensity of sunlight reaching the surface. This parameter gives one idea about the length of the path of the solar radiation through the atmosphere.

The intensity and spectral distribution of the solar radiation depends on the geographic location, date and time of the year, climate conditions, composition of the atmosphere, altitude, and many other factors. For this reason, the AM 1.5 spectral distributions are only reference estimations that provide a way to evaluate and compare the PV devices.

The AM 1.5 distributions are used as standards in the PV industry. Datasheets generally specifies the characteristics and performance of PV devices with respect to the so-called standard test condition (STC), which establishes an irradiation of 1000 W/m^2 with an AM 1.5 spectrum at 25 ◦C [30].

The solar spectrum at AM 1.5 shown in the Figure 5-3 and is comprised of 2% for UV, 54% for the visible spectrum and 44% for infrared [31].

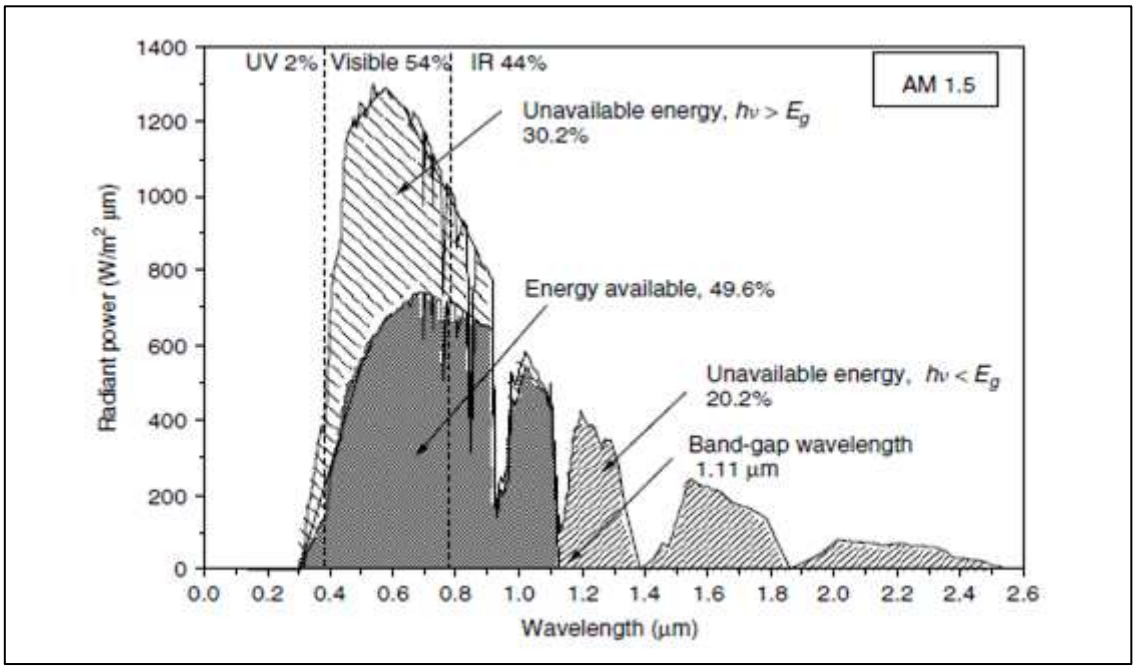

Figure 5-3 Solar spectrum at AM 1.5 [31]

5.3.4 Band-Gap Impact on Photovoltaic Efficiency

By knowing the solar spectrum and the band-gap and wavelength for silicon is possible to estimate the energy loss in a PV cell. Figure 5-3 shows the analysis for an air mass ratio of AM=1.5. As shown, 20.2% of the energy in the spectrum is lost (hv<Eg), 30.2% is also lost due absorption in the atmosphere, and the remaining 49.6% is the final portion of the solar spectrum which can be used to produce electricity by the PV cell. Therefore, energy absorption and the band-gap limit the theoretical efficiency of Si PV cells to less than 50%.

This result leads to a trade-off between selecting a PV cell with small band-gap versus one with a big band gap. Those with small band-gaps can easily establish a current but due to the excess of energy above to the threshold, its potential is wasted. Those with high band-gap limit the capacity to produce a current through the PV cell but at the same time produce a higher voltage with less waste energy [31].

In summary, low band-gaps provide more current and less voltage, while high band-gaps provide less current and higher voltage. Since power is calculated as current multiplied by voltage, there must be an intermediate band-gap value between 1.2eV and 1.8 eV which will produce the highest power output and efficiency.

Apart from the band-gap energy for the PV cells, other factors affect the theoretical efficiency of a solar cell. These include:

1) Recombination property which affects the current contribution.
2) Internal resistance of the cell.
3) Incident photons which are not absorbed by the PV cell. This could be for the following reasons: they are reflected by the PV cell's surface, they pass through the PV cell or they are blocked by the metal conductors located at the top of the PV cell.
4) A case where the voltage across the PV cell terminal is about half to two-thirds of the full band-gap voltage [31].

The efficiency of most of PV cells is low, ranging from 2% to 20% depending on the material and structure of the device. A 40% of efficiency could be potentially reached by using multilayer solar cells [2].

5.4 PV CELL MODEL

The most commonly used model for a PV cell is the one-diode equivalent circuit shown in Figure 5-4. This equivalent circuit contains a current source with a parallel diode. Additionally, parasitic resistances, series ($R_{S;}$ small) and shunt (R_{SH}, relatively large) are part of the equivalent circuit. The value of R_S varies due to factors such as the bulk resistance of the semiconductor material, metallic contacts, and interconnections, whereas R_{SH} changes mainly with the p-n junction nonidealities and impurities near the junction [26].

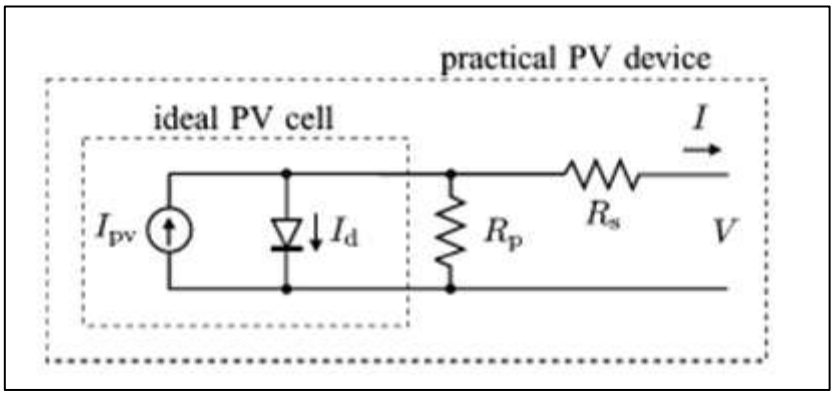

Figure 5-4 Solar cell equivalent circuit [30]

The current-voltage characteristic of a solar cell is described by the following equations:

$$I = I_{pv} - I_d \tag{5.1}$$

$$I = I_{pv} - I_0 \left[exp\left(\frac{q(V+IR_s)}{AKT}\right) - 1 \right] - \frac{V+IR_s}{R_p} \tag{5.2}$$

Where:

I_{pv} =photo current (A)

I_d = diode current (A)

I_0 = saturation current (A)

A = the diode quality constant (when T = 28 °C, A = 28)

q = electronic charge ($1.6x10^{-9}$ C)

K = Boltzmann's gas constant ($1.38\ x10^{-23}$)

T = cell temperature (°C)

R_s = series resistance (Ω)

R_p = shunt resistance (Ω)

I_L = cell current (A)

V = cell voltage (V) [32].

Equation (5.1) assumes that there is no current passing through R_{SH} (ideal cell). By doing this the net current, *I*, will be composed of the light-generated current I_{pv} and the diode current I_d. Figure 5-5 shows the nonlinear characteristic between the cell voltage and cell current represented by the solar cell equivalent circuit.

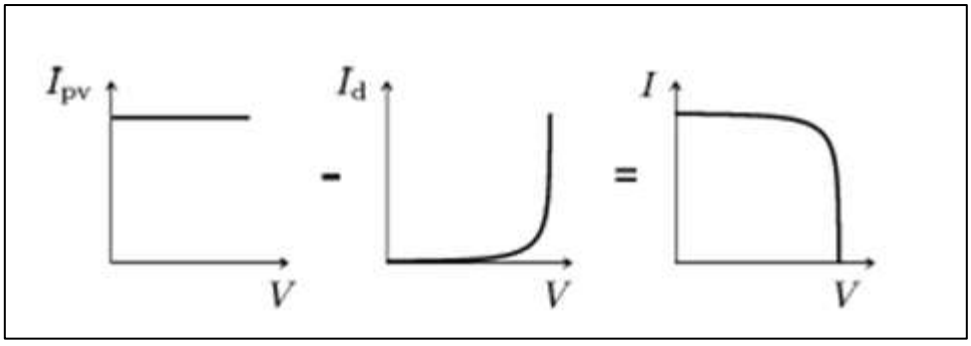

Figure 5-5 Solar cell equivalent circuit [30]

From equations (5.1) and (5.2) the I-V and P-V curves of a practical PV device can be produced, as show in Figure 5-6, where some significant points are highlighted. The short

circuit point (0, Isc), the open circuit point (Voc,0) and the Maximum Power Point (MPP) are highlighted in the Figure 5-6. The voltage and current in the MPP are known as Vmpp and Impp respectively.

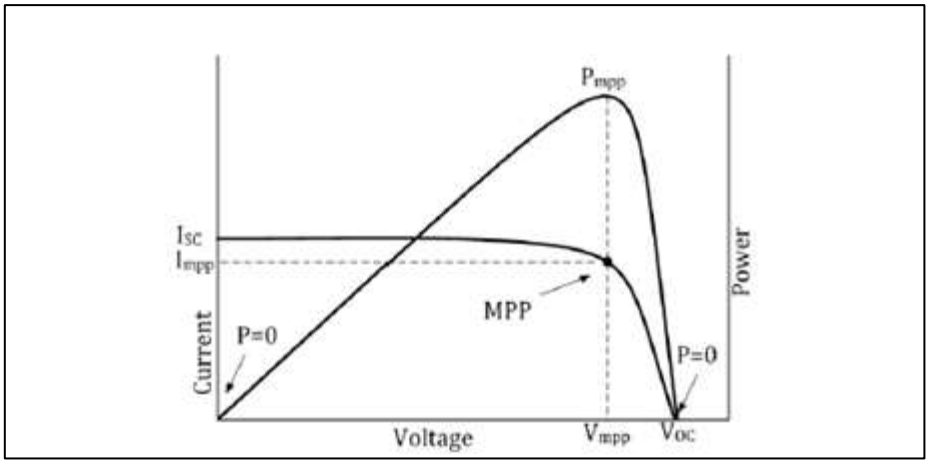

Figure 5-6 Characteristic I-V and P-V curves of a PV device

5.4.1 Factors Affecting PV Characteristic Curves

The I-V and P-V curves change as the insolation level and temperature change as shown in Figure 5-7. By increasing the insolation levels, the open circuit voltage increases logarithmically and the short circuit (I_{SC}) increases linearly. By increasing the temperature of the solar cell, the open circuit voltage (V_{OC}) decreases while the short circuit current increases slightly [26].

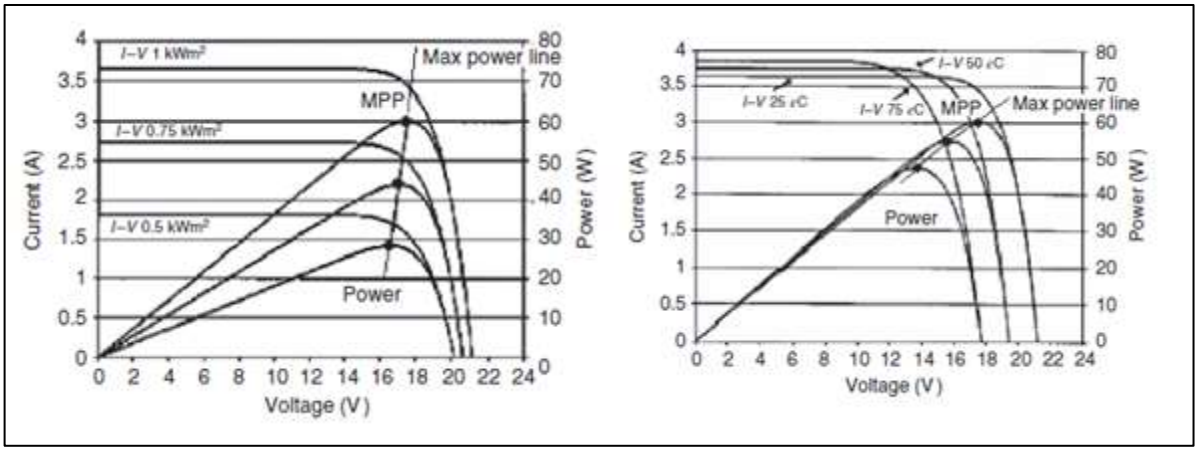

Figure 5-7 Solar cell insolation and temperature characteristics [26]

5.4.2 Maximum Power Point Tracking (MPPT)

Many PV systems use a power electronic boost converter to control the output of the PV cells by applying a bias voltage to the diode. The boost converter in Figure 5-8 is responsible for extracting the maximum power available in the solar PV system, by using a MPPT algorithm to match the output of a PV generator to a variable load [26]. The MPPT will control the duty cycle of the boost converter to maintain a constant output voltage in the converter even with variations in the solar PV system output or load changes [32].

The two most commonly used MPPT algorithms applied are the Perturb and Observe (P&O) and Incremental Conductance (IC). The main goal of MPPT is to perform impedance matching by controlling the output voltage in the solar PV system which is done by varying the duty cycle of the Pulse Width Modulation (PWM) in the DC-DC boost converter switching [33].

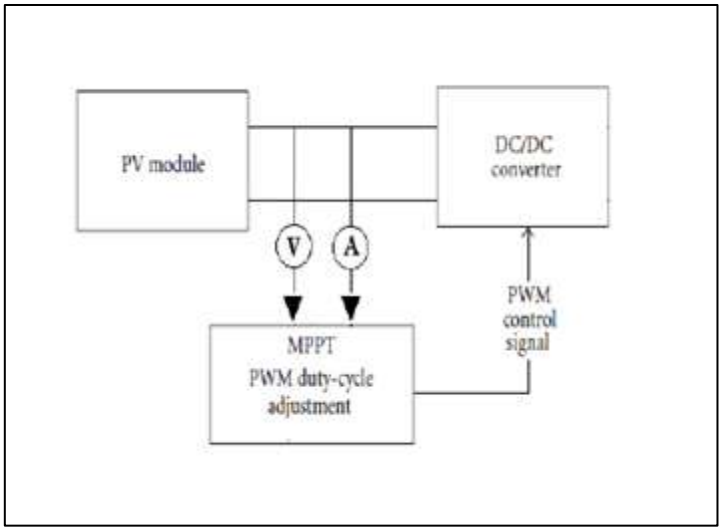

Figure 5-8 Maximum power extraction operation [33]

The P&O algorithm is widely used in PV systems because of its simplicity and ease of implementation. It operates by periodically perturbing the terminal voltage associated with the solar PV system and comparing the resulting output power with the previous output power obtained before the perturbation. If the output power increases with the perturbation, the algorithm continues in the same direction. If the output power decreases the algorithm moves in the opposite direction. Once the MPP is reached, the operating point oscillates around it [33]. However, there are some limitations with the P&O algorithm, such as, oscillations around the MPP in steady state, slow response speed, and incorrect tracking under rapid changes in weather conditions. Therefore, this method is recommended where weather conditions are changing slowly. The Figure 5-9 shows the flow chart of P&O algorithm.

The IC algorithm (Figure 5-10) can overcome some of the drawbacks of the P&O algorithm, but its implementation is more complex. This method is based on the fact that the derivative of the power with respect to the voltage (dp/dv) is equal to zero at the MPP. The ICT algorithm detects the MPP by comparing di/dv against −I/V until it reaches the voltage operating point at which the incremental conductance is equal to the source conductance.

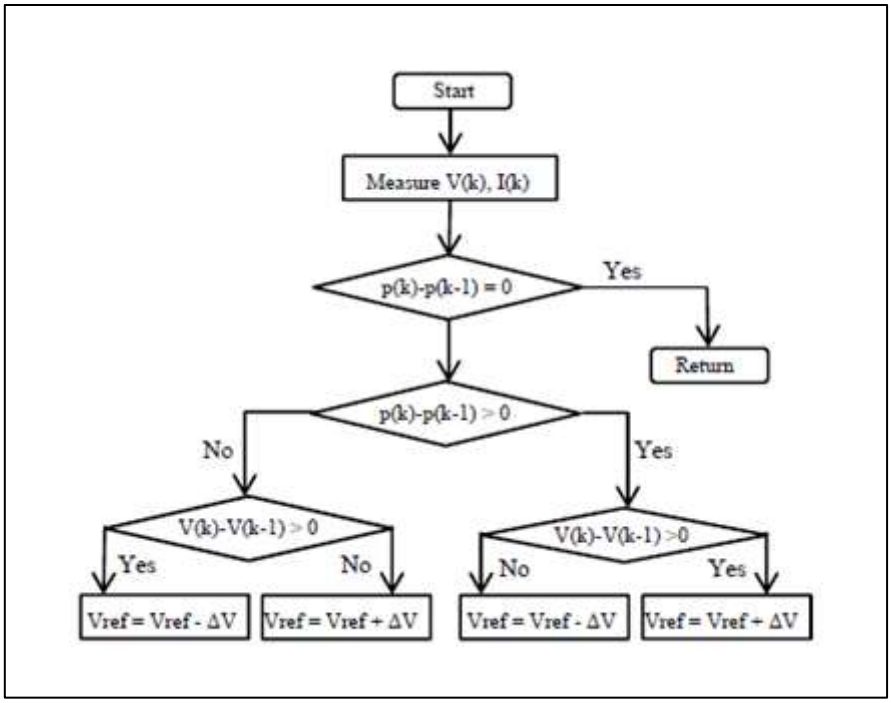

Figure 5-9 P&O flowchart [33]

The algorithm starts by measuring the present values of the I and V and proceeds to compare them with corresponding stored values (Ib and Vb) measured during the previous cycle to compute incremental changes as: dI = I −Ib and dV = V −Vb. Based on the result obtained, the control reference signal Vref will be adjusted in order to move the solar PV system voltage toward the MPP voltage. At the MPP, di/dv = −I/V; therefore, no control action is required, and the adjustment stage will be bypassed, and the algorithm will update the stored parameters at the end of the cycle. In order to detect any variation in weather conditions, the algorithm evaluates whether a control action took place when the PV array was operating at the previous cycle MPP (dv =0). This technique makes this algorithm more accurate and well suited for rapid changes in atmospheric conditions [26].

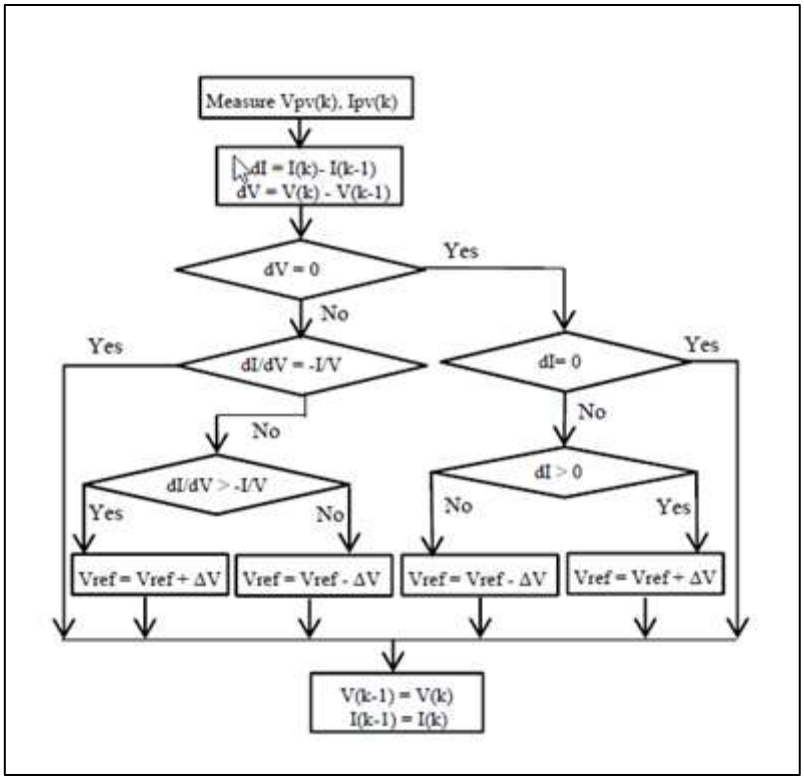

Figure 5-10 IC flowchart [33]

5.5 TEST PROCEDURE AND EQUATIONS

A test procedure was developed to determine power and energy capabilities of the two candidate PV cells for the stand-alone application.

5.5.1 Solar Irradiation measurements

A measurement of solar irradiance was used to provide a reference input that is the same as seen at the surface of the solar panel. A pyranometer was settled next to the PV system. A pyranometer is a radiometer designed for measuring the total irradiance on a plane surface which considers radiant fluxes in the wavelength range from 300 nm to 3000 nm [34].

In this case a pyranometer model CMP10 [34] was used to measure the solar irradiance or also called insolation which units are in Watts per square meter (W/m^2).

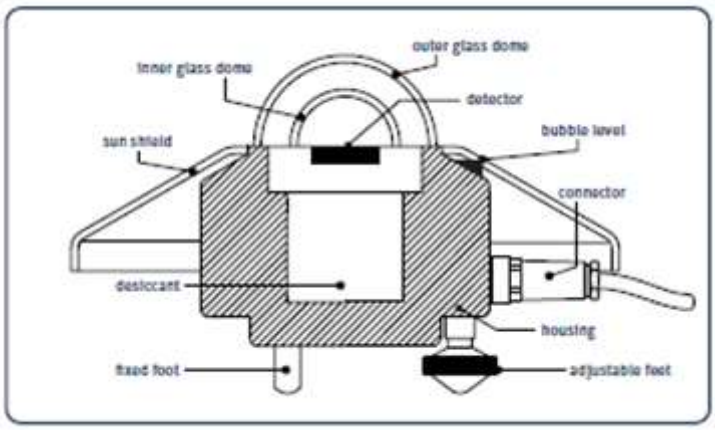

Figure 5-11 CMP10 pyranometer elements [34]

To calculate the solar irradiation, the analog output voltage of the pyranometer was applied in the following equation:

$$E_{Solar} = \frac{U_{emf}}{S} \tag{5.3}$$

Where:

E_{Solar}: Irradiance (W/m^2)

U_{emf}: Output Voltage (µV)

S: Sensitivity $\left(\frac{\mu V}{W/m2}\right)$

5.5.2 I-V and P-V Characteristic Tests

The purpose of this test was to determine the PV module's parameters such as MPP, Voc, Isc, Vmp, Imp, η and FF and also plot the I-V and P-V curves. Where:

MPP: Maximum Power Point.

Voc: Open circuit voltage.

Isc: Short circuit current.

Vmpp: Voltage at MPP.

Impp: Current at MPP.

η: PV efficiency.

FF: Fill Factor.

To obtain these parameters the following tests were conducted on different dates and times of day to assess the PV cell performance, and ultimately provide data to see if these PV cells will work for the application.

1) Open Circuit Test:

The purpose of this test is to obtain the maximum voltage (Voc) that the PV cell might provide when the terminals are not connected to any load. Since power is the product of current and voltage, no power is delivered by the cell during this test. To measure the Voc, a multimeter was connected on the PV system terminals. Figure 5-12 shows the connection on the left.

2) Short Circuit Test:

The purpose of this test is to obtain the maximum current (Isc) provided by the PV cell when its terminals are shorted together to create a short circuit condition. Similar to the open circuit test, no power is delivered by the cell during the short circuit test. To measure Isc, an ammeter was connected on the PV system terminals. Figure 5-12 shows the connection in the middle.

3) Loaded Test:

When a load is connected, some combination of current and voltage will result, and power will be delivered from the PV cell. The purpose of this test is to find the MPP, which represents the point where the PV cell produces the maximum output power (Pmpp) at a specific level of solar irradiance. The MPP is located at the knee of the I-V curve as shown at Figure 5-6.

To build the I-V and P-V curves, the load was increased progressively, and the voltage and current values were recorded. In this test, a variable resistive load (potentiometer) was used. The load values implemented were: 10 Ω, 50 Ω, 100 Ω, 150 Ω, 200 Ω, 250 Ω, 300 Ω, 400 Ω, 500 Ω, 750 Ω, 1 kΩ, 1.5 kΩ, 2 kΩ, 5 kΩ, 7.5 kΩ, 10 kΩ and 11.1 kΩ. Figure 5-12 shows the connection on the right. The results of these measurements are presented in Section 5.5.7 of this report.

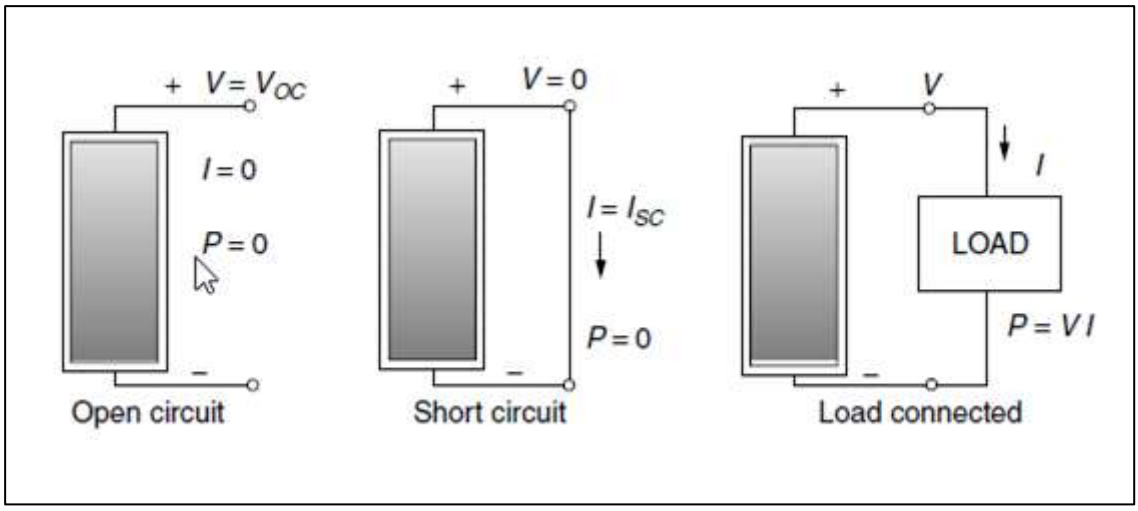

Figure 5-12 PV cell electrical test circuit connections [31]

5.5.3 Determining PV efficiency

Efficiency in photovoltaic solar panels is measured by the ability of a panel to convert sunlight into electrical energy. The efficiency is an important parameter to assess photovoltaic systems which also allows selection of a PV system adequate for the application.

The efficiency (η) of a solar photovoltaic cell is given by equation (5.4).

$$\eta = \frac{Pmp}{S*A_c} \tag{5.4}$$

Where:

Pmp: PV module's rated maximum power (W).

S: Solar radiation (W/m^2)

AC: Area of the PV cell (m^2)

5.5.4 Determining the Fill Factor

The fill factor (FF) represents a measure of the junction quality and series resistance of a PV cell. The FF is defined as the ratio between the product generated by $V_{mp}xI_{mp}$ and the one by $V_{OC}xI_{SC}$ as shown in (5.5). A FF closer to unity defines a high-quality PV cell [26].

$$FF = \frac{V_{mp}*I_{mp}}{V_{OC}*I_{SC}} \tag{5.5}$$

5.5.5 Equipment and Apparatus Required for Testing

The following equipment was used during the PV testing process.

- Kipp &Zonen Pyranometer Model CMP 10
- 2 Fluke 289 Multimeters
- 1 Fluke 287 Multimeter
- 1 Variable resistance (1Ω-10kΩ)

- 2 Solar Panels (with area of 0.006 m^2)

5.5.6 Testing Location

The measurements were performed first on the roof of the Gauss Johnson Laboratory and then near the east entrance to the second floor of the Natural Resources building, both on the University of Idaho campus. Figure 5-13 shows locations.

Figure 5-13 Measurements location

5.5.7 Test Results

Tables 5-1 and 5-2 shows the results obtained during the test procedures of the new and old solar panels.

According to the tables, the following conclusions and observations can be drawn:

- The newer cell showed better performance than the old cell in the Fall and Spring test seasons, but no as well in the Winter.
- Omitting the night measurements, the newer PV cell had a calculated efficiency ranging between 0.1% to 11.09%. For the old PV cell, the efficiency values were between 0.48% and 5.55%.

- The measurements made at night showed better performance for the old PV cell for measurements on 3/16/2017 and 4/19/2017.
- The maximum power obtained by the PV cells were 392.5 mW for the new PV cell and 215.66 mW for the old cell.
- The new cell produced higher currents values and slightly lower voltage values when compared to the old PV cell.
- Note that the measurements were not made at the same time for both PV cells, so the applied solar radiation seen for each one could be different due to the stochastic nature of the solar resource. But the pyranometer provided a reference for the efficiency calculations.

Table 5-1 Testing Values New PV Cell

Season	Date/Time	Weather Conditions	Temperature	Humidity	Air Speed	Voc (V)	Isc (mA)	Vmpp (V)	Impp (mA)	Pmpp (mW)	η (%)	FF	Notes
Fall	10/8/2016 4:27 PM	Partly Sunny	62°F	58%	14 m.p.h	5.34	15.02	3.67	9.15	33.58	5.50	0.42	
	11/22/2016 1:00 PM	Partly Sunny	47°F	62%	10 m.p.h ESE	5.86	21.23	4.49	14.85	66.68	6.33	0.54	
Winter	1/26/2017 10:00 AM	Cloudy/ Cloud cover 93% **Without Snow**	30°F	86%	1 m.p.h SSE	5.42	14.19	3.64	9.04	32.89	4.25	0.43	
	1/26/2017 10:29 AM	Cloudy/ Cloud cover 93% **With Snow**				3.16	3.73	1.38	1.84	2.55	0.65	0.22	
	1/26/2017 12:16 PM	Mostly Cloudy/ Cloud cover 91% **Without Snow**	30°F	83%	2 m.p.h S	5.85	23.23	4.26	16.906	72.02	5.75	0.53	
	1/26/2017 12:03 PM	Mostly Cloudy/ Cloud cover 91% **With Snow**				4.44	7.07	2.76	4.24	11.70	2.29	0.37	
	1/27/2017 9:00 AM	Fog/ Cloud cover 97% **Without Snow**	24°F	92%	8 m.p.h E	4.95	10.16	3.14	6.24	19.62	2.53	0.39	
	1/27/2017 9:18 AM	Fog/ Cloud cover 97% **With Snow**				3.07	3.63	2.04	2.72	5.55	1.01	0.50	
	1/27/2017 12:07 PM	Cloudy/ Cloud cover 95% **Without Snow**	32°F	84%	9 m.p.h E	6.06	35.89	5.00	24.85	124.25	5.27	0.57	
	1/27/2017 11:53 AM	Cloudy/ Cloud cover 95% **With Snow**				5.30	12.69	3.74	7.43	27.79	3.10	0.41	
	1/27/2017 3:54 PM	**Without Snow**				3.081	3.637	1.72	1.71	2.94	0.99	0.26	Missing Weather conditions
	1/27/2017 4:08 PM	**With Snow**				0.87	0.73	0.39	0.39	0.15	0.10	0.24	Missing Weather conditions
	2/13/2017 8:36 AM	Intermittent Clouds Cloud cover 61%	28°F	76%	9 m.p.h E	4.29	8.59	1.83	7.64	13.98	2.00	0.38	
	2/13/2017 11:57 AM	Intermittent Clouds Cloud cover 56%	39°F	61%	12 m.p.h E	5.99	65.12	4.9	48.33	236.82	6.83	0.61	
	2/13/2017 4:05 PM	Mostly Sunny Cloud cover 10%	41°F	60%	5 m.p.h ESE	2.85	3.31	1.43	1.9	2.72	1.00	0.29	

Table 5-1 Testing Values New PV Cell (continuation)

Season	Date/Time	Weather Conditions	Temperature	Humidity	Air Speed	Voc (V)	Isc (mA)	Vmpp (V)	Impp (mA)	Pmpp (mW)	η (%)	FF	Notes
Spring	3/16/2017 8:38 AM	Partly Sunny/ Cloud cover 35%	39°F	83%	13 m.p.h WSW	4.53	7.96	3.20	4.27	13.67	2.78	0.38	
	3/16/2017 12:21 PM	Partly Sunny/ Cloud cover 45%	44°F	71%	18 m.p.h WSW	5.54	40.00	4.83	20.11	97.15	4.91	0.44	
	3/16/2017 3:51 PM	Partly Sunny/ Cloud cover 46%	47°F	58%	16 m.p.h WSW	5.84	58.42	4.56	44.89	204.65	6.67	0.60	
	3/16/2017 6:57 PM	Mostly clear/ Cloud cover 26%	41°F	71%	8 m.p.h W	0.421	0.332	0.095	0.126	11.970	0.0095	0.09	Nota 1: Pmpp in uW
	3/16/2017 7:15 PM	Mostly clear/ Cloud cover 26%	41°F	71%	8 m.p.h W	0.020	0.015	0.003	0.008	0.026	0.00005	0.09	Nota 1: Pmpp in uW
	4/19/2017 8:40 AM	Mostly Sunny/ Cloud cover 27%	44°F	0.63	8 m.p.h E	5.75	41.96	4.61	30.38	140.06	5.19	0.58	
	4/19/2017 12:02 PM	Partly Sunny/ Cloud cover 34%	57°F	48%	10 m.p.h ESE	5.76	108.61	4.53	86.74	392.50	7.53	0.63	
	4/19/2017 4:02 PM	Cloudy/ Cloud cover 99%	61°F	33%	9 m.p.h E	5.63	46.43	3.98	39.75	158.15	8.51	0.61	
	4/19/2017 7:30 PM	Showers/ Cloud cover 90%	56°F	48%	8 m.p.h ESE	0.89	0.76	0.315	0.314	98.91	0.10	0.15	Nota 1: Pmpp in uW
	4/19/2017 8:35 PM	Cloudy/ Cloud cover 99%	50°F	65%	10 m.p.h NNE	2.04	1.42	0.974	0.83	0.81	1.22*10^-6	0.28	Nota 2: Pmpp in nW, Voltages in mV and
	5/19/2017 8:33 AM	Partly Sunny/ Cloud cover 31%	52°F	71%	4 m.p.h SE	5.77	55.17	4.40	43.30	190.43	5.79	0.60	
	5/19/2017 11:56 AM	Partly Sunny with showers/ Cloud cover 27%	63°F	53%	4 m.p.h N	5.40	35.62	5.23	36.96	193.42	11.09	1.01	
	5/19/2017 3:55 PM	Partly Sunny/ Cloud cover 39%	65°F	45%	5 m.p.h N	5.58	103.10	4.29	81.80	350.51	7.28	0.61	

Notes: The Fill factor was calculated based on the Voc and Isc measured since the nominal characteristic of the PV cell were not available

Table 5-2 Testing Values Old PV Cell

Season	Date/Time	Weather Conditions	Temperature	Humidity	Air Speed	Voc (V)	Isc (mA)	Vmpp (V)	Impp (mA)	Pmpp (mW)	η (%)	FF	Notes
Fall	10/8/2016 4:50 PM	Partly Sunny	62°F	58%	14 m.p.h	5.4	7.12	2.46	7.17	33.91	5.55	0.46	
	11/22/2016 1:20 PM	Partly Sunny	47°F	62%	10 m.p.h ESE	5.99	12.2	4.47	11.11	49.66	4.61	0.68	
Winter	1/26/2017 10:11 AM	Cloudy/ Cloud cover 93% **Without Snow**	30°F	86%	1 m.p.h SSE	5.83	8.55	4.32	8.64	37.34	4.82	0.75	
	1/26/2017 10:19 AM	Cloudy/ Cloud cover 93% **With Snow**				4.96	1.98	3.71	1.86	6.89	2.24	0.70	
	1/26/2017 12:14 PM	Mostly Cloudy/ Cloud cover 91% **Without Snow**	30°F	83%	2 m.p.h S	6.26	14.17	4.84	12.04	58.29	4.55	0.66	
	1/26/2017 12:08 PM	Mostly Cloudy/ Cloud cover 91% **With Snow**				5.57	4.34	3.91	3.90	15.26	3.08	0.63	
	1/27/2017 9:07 AM	Fog/ Cloud cover 97% **Without Snow**	24°F	92%	8 m.p.h E	5.70	6.94	4.07	6.23	25.34	3.62	0.64	
	1/27/2017 9:14 AM	Fog/ Cloud cover 97% **With Snow**				5.01	1.74	3.36	1.68	5.65	1.22	0.65	
	1/27/2017 12:03 PM	Cloudy/ Cloud cover 95% **Without Snow**	32°F	84%	9 m.p.h E	6.50	23.99	5.18	20.60	106.73	4.41	0.69	
	1/27/2017 11:58 AM	Cloudy/ Cloud cover 95% **With Snow**				5.94	6.95	4.88	6.49	31.65	3.41	0.77	
	1/27/2017 3:59 PM	**Without Snow**				5.11	1.89	3.22	1.61	5.19	1.77	0.54	Missing Weather conditions
	1/27/2017 4:05 PM	**With Snow**				4.13	0.38	2.90	0.29	0.84	0.48	0.54	Missing Weather conditions
	2/13/2017 8:41 AM	Intermittent Clouds Cloud cover 61%	28°F	76%	9 m.p.h E	5.56	6.61	4.2	5.56	23.35	2.28	0.64	
	2/13/2017 11:52 AM	Intermittent Clouds Cloud cover 56%	39°F	61%	12 m.p.h E	6.21	32.88	4.62	30.31	140.03	4.03	0.69	
	2/13/2017 4:08 PM	Mostly Sunny Cloud cover 10%	41°F	60%	5 m.p.h ESE	4.97	1.95	3.43	1.71	5.87	2.32	0.61	

Table 5-2 Testing Values Old PV Cell (continuation)

Season	Date/Time	Weather Conditions	Temperature	Humidity	Air Speed	Voc (V)	Isc (mA)	Vmpp (V)	Impp (mA)	Pmpp (mW)	η (%)	FF	Notes
Spring	3/16/2017 8:44 AM	Partly Sunny/ Cloud cover 35%	39°F	83%	13 m.p.h WSW	5.48	5.90	4.34	4.35	18.86	3.57	0.58	
	3/16/2017 12:27 PM	Partly Sunny/ Cloud cover 45%	44°F	71%	18 m.p.h WSW	5.75	16.40	4.56	11.23	51.24	3.95	0.54	
	3/16/2017 3:57 PM	Partly Sunny/ Cloud cover 46%	47°F	58%	16 m.p.h WSW	6.04	29.86	4.94	24.52	121.20	4.03	0.67	
	3/16/2017 7:05 PM	Mostly clear/ Cloud cover 26%	41°F	71%	8 m.p.h W	2.84	0.08	0.312	0.032	9.984	0.0104	0.05	Nota 1: Pmpp in uW
	3/16/2017 7:10 PM	Mostly clear/ Cloud cover 26%	41°F	71%	8 m.p.h W	0.612	0.003	0.015	0.003	0.044	0.00011	0.02	Nota 1: Pmpp in uW
	4/19/2017 8:45 AM	Mostly Sunny/ Cloud cover 27%	44°F	0.63	8 m.p.h E	6.13	31.09	4.42	29.04	128.37	4.57	0.67	
	4/19/2017 12:08 PM	Partly Sunny/ Cloud cover 34%	57°F	48%	10 m.p.h ESE	5.88	54.71	4.62	46.70	215.66	4.26	0.67	
	4/19/2017 4:07 PM	Cloudy/ Cloud cover 99%	61°F	33%	9 m.p.h E	5.70	16.60	4.26	14.17	60.29	4.47	0.64	
	4/19/2017 7:34 PM	Showers/ Cloud cover 90%	56°F	48%	8 m.p.h ESE	3.64	0.29	1.865	0.169	315.19	0.40	0.30	Nota 1: Pmpp in uW
	4/19/2017 8:42 PM	Cloudy/ Cloud cover 99%	50°F	65%	10 m.p.h NNE	305.17	0.99	10.739	0.96	10.31	1.6946E-05	0.03	Nota 2: Pmpp in nW, Voltages in mV and
	5/19/2017 8:38 AM	Partly Sunny/ Cloud cover 31%	52°F	71%	4 m.p.h SE	6.11	39.44	4.99	32.67	162.84	4.84	0.68	
	5/19/2017 12:02 PM	Partly Sunny with showers/ Cloud cover 27%	63°F	53%	4 m.p.h N	5.58	18.40	4.08	13.39	54.65	4.83	0.53	
	5/19/2017 4:01 PM	Partly Sunny/ Cloud cover 39%	65°F	45%	5 m.p.h N	5.63	58.22	4.62	45.25	208.83	5.05	0.64	

Notes: The Fill factor was calculated based on the Voc and Isc measured since the nominal characteristic of the PV cell were not available

CHAPTER 6. CONCLUSIONS AND FUTURE WORK

6.1 CONCLUSION

Increasing DER penetration and the implementation of smart grid technologies are creating opportunities while also demanding more complex analysis and control for the distribution networks. The distribution network transformation involves the participation of federal and state stakeholders, utility companies, manufacturers and the customers in the creation of more sophisticated means of control and design challenging engineering analysis tools to enable "Distribution Grid in the 21st Century" [6]. This thesis implemented a partial VVO scheme as a solution for improving voltage stability and energy efficiency, reducing the peak demand and providing a quality service to the customers as DER penetration increases. In addition, the study of Volt-var regulation method is used as a test point in the development of resilience metrics for evaluating the availability of the assets and resources to qualify electrical system solutions for times when the bulk power system experiences disturbance conditions. This type of studies in this thesis allow the electrical system planners, designers and operators to consider more parameters in the analysis of the MDS.

The objective of this work was to develop algorithms to efficiently determine location and rating of dynamic reactive power sources. In the case of VVO, this single specific control solution requires the solving an unbalanced powerflow which contains a large set of nonlinear equations and state variables. All these requirements have made the VVO a long-standing challenge in the industry [7].

The method proposed in this work used the $Z_{BUS,}$ which was calculated in Mathcad. However, the results from the calculations did not correlate with those generated by GridLAB-D. Since the load of the system varies with the time, an accurate load modeling is needed to improve the Mathcad calculations to better match the GridLAB-D. The overhead lines and

transformers impedances were well known but the load impedances were not incorporated in the Z_{BUS}. Thus, the Z_{BUS} calculation only served as a starting point for the GridLAB-D studies.

Additionally, the incorporation of more than one inverter operating Volt-var mode in GridLAB-D had poor results due to control interactions in the models. Therefore, case A was solved by applying one inverter in Volt-var mode and a second one in constant PQ mode (injecting only Q). Case B was partially solved by applying one inverter in Volt-var mode since the connection of a SVR in the branch 2 helped to compensate the voltage more uniformly in this branch. The range A and range B of the standard ANSI C84.1 were used as references to evaluate the compensation in the system, however; for the point of view of resilience, these limits may need further consideration keep the system from operating too close to the limit conditions and leave some margin of maneuver to overcome disturbances or faults that can occur in the system. By allowing these additional margins once the reactive power is injected on the system, there will be a tradeoff between make the system more resilient versus a potentially high cost operating point.

After applying the reactive compensation approach in this thesis, a voltage stability analysis was applied at one of buses and it was demonstrated that the voltage stability limit of that bus was extended with the placement of the D-STATCOM in the system. Therefore; the system became more stable and resilient.

In the final part of this work two candidate solar panels were tested for a stand-alone application. The new solar panel was more efficient and had a higher peak output.

6.2 FUTURE WORK

6.2.1 Secondary Voltage Regulation

High levels of DERs in the distribution networks have resulted in the elevation of the voltages levels in distribution systems, secondary voltage regulation represents a potential resource to allows the deployment of these non-dispatchable sources by using the Volt-var control mode in the smart inverters can improve margin to maneuver to respond to extreme conditions. This thesis did preliminary work in this. A next step would be to both increase DER penetration and evaluate options for many small smart inverters or a few larger ones.

6.2.2 Impact of Distribution System Operations on Transmission Systems

One of the key issues surrounding the analysis of smart grid technologies is how to maximize the value of deployed assets. By assessing locally, the benefits of such assets may underestimate their global contribution into the EPS. The installation of shunt D-STATCOMs to improve the voltage profile on a distribution feeder will reduce the demand of reactive power from the transmission system. Also, the high penetration of DERs on distribution levels will impact the operational characteristics of the transmission levels [25]. The electrical analysis from this work needs to be extended to the transmission levels to see the impact of the distribution network operation on the high voltage side.

6.2.3 Energy Storage and Wind Generation

Since the wind generation and energy storage represents additional generation resources to be incorporate on the MDS, further studies could evaluate the impact of each on resilience and stability of the system. GridLAB-D allows to model these new assets.

6.2.4 Electrical Analysis for Other Types of Economic Units

Since this thesis studied only the residential EU; the reactive power compensation for urban, rural and industrial EUs will provide insight into the future challenges faced by the MDS. By considering meshed and semi-meshed topologies and different types of loads, more scenarios could be evaluated, and more information will be provided to compute the resilience metrics.

6.2.5 Load modeling and Multi Volt-var devices

There are several problems from the work in this thesis that need to be corrected, including the modeling of the time varying load to better align the results obtained in Mathcad and GridLAB-D. In addition, a solution for the operation of multi Volt-var devices to reach correct solutions for the cases proposed in this thesis. Smart inverters have integrated Volt-var function and with the deployment of these devices a realistic simulation should allow the operation of many of them in the distribution system. One important scenario is to evaluate the distributed placement of small D-STATCOMs to compare the results with the more centralized solutions presented in this thesis. To better perform these studies, it would be a great benefit to be able to extract the Y_{BUS} from GridLAB-D and evaluate it directly.

6.2.6 Resilience Metrics

The proposed method represents a starting point to determine possible deployment of dynamic reactive devices such as D-STATCOMs in distribution systems. To fully assess the impact of this compensation, resilient metrics can be calculated based on the amount of reactive power injected in the system and the improvement voltage sensitivities for the system. Since the results in this thesis are in steady-state, transient behavior of D-STATCOM also is

needed to evaluate the time of response when the system is facing abnormal conditions, which represents an important parameter also to evaluate the resilience of the system.

6.2.5 PV Cell Testing

More tests are required for the whole system of small stand-alone lighting application to have a more accurate estimation about the ability of PV solar-battery system to supply the lighting, processing and communication load in all seasons of the year and a variety of weather conditions. The batteries need to be tested to determine the charging and discharging times then round-trip efficiency, and the impact of the temperature in their performance. The test method for the complete system should be formalized to provide an efficient approach to evaluate new subsystems such as new PV cells, new processors, and so on.

.

REFERENCES

[1] Mahmud, N., and Zahedi, A. "Review of control strategies for voltage regulation of the smart distribution network with high penetration of renewable distributed generation," *Renewable and Sustainable Energy Reviews*, 64, 582-595. 2016.

[2] Rashid, M. *Power electronics: Circuits, devices, and applications* (4th ed.). Upper Saddle River, N.J.: Pearson/Prentice Hall. 2014.

[3] Uluski, B. *Volt/var control and optimization concepts and issues*. Electric Power Research Institute (EPRI), p. 58. 2011.

[4] Gupta, A. R., and Kumar, A. "Optimal placement of D-STATCOM using sensitivity approaches in mesh distribution system with time variant load models under load growth," *Ain Shams Engineering Journal*, 2016, pp. Ain Shams Engineering Journal.

[5] Taft, J. D., De Martini, P., and Kristov, L. *A reference model for distribution grid control in the 21st century* (No. PNNL-24463). Pacific Northwest National Laboratory (PNNL), Richland, WA (United States). 2015.

[6] De Martini, P., and Kristov, L. "Distribution Systems in a High Distributed Energy Resources Future: Planning, Market Design, Operation and Oversight," *Future Electric Utility Regulation series. Lawrence Berkeley National Laboratory*. 2015

[7] National Electrical Manufacturers Association. Volt/VAR optimization improves grid efficiency. Available: *https://www.nema.org/Policy/Energy/Smartgrid/Documents/VoltVAROptimazation-Improves% 20Grid-Efficiency. Pdf*, accessed on: 11/20/2017.

[8] National Electrical Manufacturers Association, *ANSI C84.1 Electric Power Systems and Equipment – Voltage Ratings (60 Hertz)*, [online] Available: www.nema.org/stds/c84-1.cfm, accessed on: 11/27/2017.

[9] Kersting, W. H. *Distribution System Modeling and Analysis*. 2nd edition, Boca Raton: CRC Press, 2007.

[10] Borozan, V., Baran, M., and Novosel, D., "Integrated Volt/Var Control in Distribution Systems," *IEEE Power Engineering Society Winter Meeting*, vol. 3, 2001, pp. 1485-1495. Columbus, OH, USA.

[11] Pinney, D. *Costs and benefits of conservation voltage reduction*. National Rural Cooperative Association, Arlington, VA, Tech. Rep. 2013

[12] Basso, T. *IEEE 1547 and 2030 standards for distributed energy resources interconnection and interoperability with the electricity grid*. No. NREL/TP-5D00-63157. National Renewable Energy Laboratory (NREL), Golden, CO., 2014.

[13] *IEEE Standard for Interconnecting Distributed Resources with Electric Power Systems*, IEEE Std 1547-2003, vol., no., pp.1-28, July 28 2003.

[14] *IEEE Standard for Interconnecting Distributed Resources with Electric Power Systems - Amendment 1,* in IEEE Std 1547a-2014 (Amendment to IEEE Std 1547-2003, vol., no., pp.1-16, May 21 2014.

[15] Parker, W., Johnson, B. K., McJunkin, T. R. and Rieger, C.G. "Identifying Critical Resiliency of Modern Distribution Systems with Open Source Modeling," *IEEE Resilience Week 2017*. Wilmington, DE, USA. 2017.

[16] McJunkin, T. R., and Rieger, C. G. "Electricity distribution system resilient control system metrics," *Resilience Week (RWS), 2017* (pp. 103-112). Wilmington, DE, USA. 2017.

[17] Eshghi, K., Johnson, B. K., and Rieger, C. G. "Power system protection and resilient metrics," *Resilience Week (RWS), 2015* (pp. 1-8). IEEE. Philadelphia, PA, USA 2015.

[18] Grid Lab-D Simulation Software, Available: http://www.gridlabd.org/, accessed on 11/27/2017.

[19] Chassin, D. GridLAB-D Tutorial- Session 2 Power Flow Module. Available: https://github.com/dchassin/tutorial/blob/master/Session%202/Tutorial%202.pdf, accessed on: 11/20/2017.

[20] P. A. N. Garcia, J. L. R. Pereira, S. Carneiro Jr., V. M. Da Costa, and N. Martins, "Three-Phase Power Flow Calculations using the Current Injection Method," *IEEE Transaction on Power Systems, Vol. 15, Issue 4, May 2000*, pp. 508-514.

[21] Wilcox, S. and Marion, W. *Users Manual for TMY3 Data Sets*. National Renewable Energy Laboratory, Golden, CO, Rep. TP-581-43156 May 2008.

[22] Commercial and Residential Hourly Load Profiles for all TMY3 Locations in the United States [Online] Available: http://en.openei.org/doe-opendata/dataset/commercial-and-residentialhourly-load-profiles-for-all-tmy3-locations-in-the-united-states. Accessed Oct 29, 2017.

[23] GridLAB-D™ A Unique Tool to Design the Smart Grid [Online] Available: http://www.gridlabd.org/brochures/20121130_gridlabd_brochure.pdf. Accessed Nov 15, 2017.

[24] Kundur, P. *Power System Stability and Control*. McGraw-Hill Inc, 1993.

[25] Schneider, K. P., Fuller, J. C., Tuffner, F. K., & Chen, Y. *Modern Grid Strategy: Enhanced GridLAB-D Capabilities Final Report* (No. PNNL-18864). Pacific Northwest National Laboratory (PNNL), Richland, WA (US). 2009.

[26] Rashid, M. H. *Power electronics handbook: devices, circuits and applications*. Elsevier Inc. 2011.

[27] GridLAB-D resources [Online] Available: http://gridlab-d.sourceforge.net/wiki/index.php/Main_Page . Accessed Nov 27, 2017.

[28] Glover, J., Sarma, Mulukutla S., and Overbye, Thomas J. *Power system analysis and design* (5th ed.). Stamford, CT: Cengage Learning. 2012.

[29] Kundur, P. et al., "Definition and classification of power system stability IEEE/CIGRE joint task force on stability terms and definitions," *IEEE Transactions on Power Systems*, vol. 19, no. 3, pp. 1387-1401, Aug. 2004.

[30] Villalva, M., Gazoli, J., and Filho, E. "Comprehensive Approach to Modeling and Simulation of Photovoltaic Arrays," *IEEE Transactions on Power Electronics*, Vol 24, No 5, 1198-1208. 2009

[31] Masters, G. *Renewable and efficient electric power systems*. Hoboken, NJ: John Wiley & Sons. 2004.

[32] Elshaer, M., Mohamed, A., and Mohammed. "Smart optimal control of DC-DC boost converter in PV systems," *Transmission and Distribution Conference and Exposition: Latin America (T&D-LA)*, 2010 IEEE/PES (pp. 403-410). 2010.

[33] Sood, V. K., and Bhalla, P. “EMTP model of grid connected PV system,” *International Conference on Power Systems Transients (IPST)*.2013.

[34] KippZonen Instruction Sheet and Brochure for Pyranometers CMP Series. [Online] Available: http://www.kippzonen.com. Accessed Oct 29, 2017.

APPENDIX A. SYSTEM DATA

The following data described the system used in Chapter 3 and 4. The information about the solar generation outputs and the load behaviors are explained with more detail in Chapter 3.

Table A-1 Distribution Lines (R and X in p.u on 20 MVA base)

Line	R	X
1-2	0.0097	0.1175
2-3	0.001	0.01
3-4	0.002	0.02
4-5	0.001	0.015
5-6	0.001	0.008
6-7	0.003	0.03
7-8	0.001	0.009
8-9	0.005	0.05
10-11	0.004	0.04
11-12	0.01	0.102
12-13	0.008	0.082
14-5	0.007	0.072
15-2	0.005	0.051
15-16	0.001	0.015
17-2	0.002	0.02

Table A-2 Transformers (R and X in p.u on 20 MVA base)

TX	R	X
TX_SE	0.00033	0.0022
TX_RES	0.1	0.3333